fluids

MDPI

Review

Droplet Contact Line Dynamics after Impact on Solid Surface: Future Perspectives in Healthcare and Medicine

Alireza Mohammad Karim

Nanoscience Centre, Department of Engineering, University of Cambridge, 11 J. J. Thomson Avenue, Cambridge CB3 0FF, UK; am2633@cantab.ac.uk

Abstract: The physics of the moving contact line of an impacting droplet is widely applied in a variety of domains in rapidly advancing healthcare technology and medicine. The behavior of the dynamic contact line after impact of a biologically active droplet on a complex material surface involves complicated solid–liquid and liquid–gas interfacial interactions. Therefore, a deep understanding of such complex droplet contact line dynamics by applying the current physical models and state-of-the-art nanotechnology and artificial neural networks can be one of the ongoing promising interests in the field of interfacial physics. This review provides an overview of several scientific aspects of contact line dynamics of an impacting droplet and its influence on the current developed healthcare technology and medicine. Firstly, the potential applications in modern healthcare and personalized medicine are listed and discussed. Secondly, the theory of the moving contact line and the fundamental physical parameters related to the motion of impacting droplets are introduced. Afterwards, the current physical models of moving contact line dynamics are critically explained by emphasizing their limitations. Finally, current concerns and obstacles are summarized, and future perspectives and research directions are outlined to address poorly understood and conflicting issues.

Keywords: droplet; contact line; contact angle; bioprinting; biosensor; personalized medicine

check for updates

Citation: Mohammad Karim, A. Droplet Contact Line Dynamics after Impact on Solid Surface: Future Perspectives in Healthcare and Medicine. *Fluids* **2024**, *9*, 223. https://doi.org/10.3390/fluids9100223

Academic Editor: Giuliano De Stefano

Received: 22 July 2024
Revised: 11 September 2024
Accepted: 23 September 2024
Published: 26 September 2024

Copyright: © 2024 by the author. Licensee MDPI, Basel, Switzerland. This article is an open access article distributed under the terms and conditions of the Creative Commons Attribution (CC BY) license (https://creativecommons.org/licenses/by/4.0/).

1. Introduction

Droplet impact is a common physical phenomenon in daily life. The frequent examples in nature are rainfall on the ground and a coffee stain. Droplet impingement on a solid surface has shown numerous applications in various scientific fields, including healthcare, medicine, aerospace, electronics, food processing, smart materials, coatings, printings, microfluidics, and nanofluidics [1–314].

The physics of droplet impact on various surfaces has been the center of attention in the scientific community during the pandemic for efficient prevention of the spread of the COVID-19 virus-laden droplets in society [234,245]. Rapidly advancing scientific and commercialization efforts around the world in state-of-the-art droplet-based bioprinting have revolutionized personalized medicine, covering various applications that include gene-expression analysis, single-cell printing, individualized diagnosis and drug therapy, and functional nanobiomaterials [85,92,96,101,105,126,152,170,178,194,215,217,218,247,289,307].

Furthermore, skin-interface wireless wearable electrochemical biosensors, which are an emerging technology, are fabricated by the innovative three-dimensional printing of bioelectrically conducting droplets on soft biocompatible materials for the possibility of real-time health surveillance. A popular example is electrochemical biosensors for peripheral biochemical, nutrition, and metabolite monitoring and control for every specific patient [260–268,312,314]. This highly precise, personalized healthcare technology is critically dependent on how accurate the active complex nano- and microbiodroplets are being deposited on the complex biocompatible and/or biodegradable elastic soft stretchable materials.

Despite more than a century of scientific study on droplet impact physics, there has not been a comprehensive understanding of this rapid physical process until the recent emergence of high-speed imaging techniques and the help of advanced computational tools [1–314]. These technologies significantly facilitate better interpretation of droplet impact physics [17,68–70,135,137,138,223,273–275,281]. The droplet impact on a solid surface consists of the following physical events: spreading and deposition, receding and breakup, prompt splash, corona splash, partial bounce, and complete bounce as shown in Figure 1 [5,16,17,52,54,98–130]. For numerous applications, such as printed electronics and smart materials for healthcare and medicine, a great understanding of droplet spreading after impact on a solid surface is the main concern for the purpose of high quality and precise functionality demands.

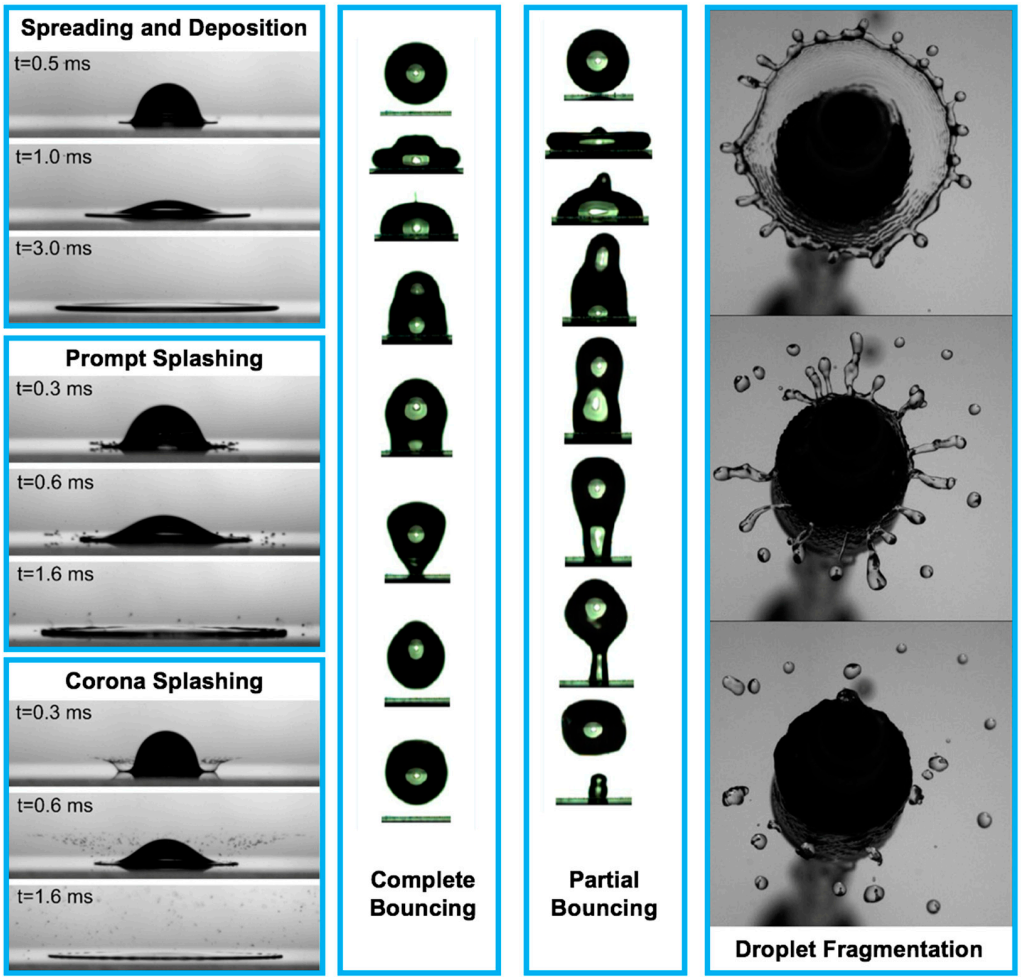

Figure 1. The physical events after droplet impact on a solid surface [11,104,253]. Reprinted from The Journal of Fluid Mechanics, 668, Villermaux, E. and Bossa, B. "Droplet fragmentation on impact", 412–435, Copyright (2011), with permission from Cambridge University Press. Reprinted from Langmuir, 33, Malla, L. K., Patil, N. D., Bhardwaj, R., and Neild, A. "Droplet bouncing and breakup during impact on a microgrooved surface", 9620–9631, Copyright (2017), with permission of American Chemical Society. Reprinted from Journal of Colloid and Interface Science, 553, Almohammadi, H. and Amirfazli, A. "Droplet impact: viscosity and wettability effects on splashing", 22–30, Copyright (2019), with permission from Elsevier. Spreading and deposition: silicone oil droplet with kinematic viscosity of 1 cSt and impact velocity of 1.4 m/s; Prompt splashing: glycerol–water droplet with kinematic viscosity of 2 cSt and impact velocity of 2.8 m/s; Corona splashing: silicone oil droplet with kinematic viscosity of 1 cSt and impact velocity of 2.5 m/s; Complete bouncing: time interval

between the first and second images is 1 ms, from second image up to sixth image, the time interval is 2 ms, and the time interval between the last three images is 1.33 ms, impact velocity is 0.52 m/s, the Weber number is 6.5, and the water droplet diameter is 1.7 mm; Partial bouncing: time interval between the first and second images is 1 ms, from second image up to sixth image, the time interval is 2 ms, and the time interval between the last three images is 1.33 ms, impact velocity is 0.82 m/s, the Weber number is 16.2, and the water droplet diameter is 1.7 mm; Droplet fragmentation: time interval between the images is 10 ms, and the Weber number is 490.

This review provides the importance of this field of science (i.e., physics of droplet spreading) on the future of personalized healthcare and medicine in a wide range of areas, including bioprinting and advanced biosensors. Next, this review provides a summary of the prominent physical factors related to droplet spreading after impact. Moreover, it presents the current physical models along with their strengths and weaknesses that can be used to explain the physics of droplet spreading in healthcare and medicine. Finally, future research directions in this field are provided, considering the complexities of the droplets and solid surfaces along with recent advancements in nanotechnology, such as atomic force microscopy, cryogenic electron microscopy, and state-of-the-art neural networks.

2. Applications: Healthcare and Medicine

2.1. Three-Dimensional (3D) Bioprinting

Depositing tiny specialized biological droplets onto biocompatible materials with complex geometry and advanced thermal and mechanical properties to fabricate highly sensitive advanced functional biological 3D structures has been of considerable research interest because of its wide range of applications in personalized healthcare technology and medicine (Figure 2a). Figure 2a depicts the multiple stages of printing an array of biological droplets on a substrate via applying the droplet-impact printing approach. The biological droplets can contain various biological solutions, such as live cells, DNA, virus, and bacteria. This technique is strongly applicable for various biomedical research, including cell culture-based studies. The coated substrate can have various wettability ranging from superhydrophilic to superhydrophobic.

It is important to emphasize that, in bioprinting technology, the size of the biological droplets is commonly in the order of tens of micrometers in diameter. This experimental procedure is known as 3D bioprinting in which the biological droplets are commonly made of active biochemicals, living cells, proteins, peptides, enzymes, hormones, etc. [69, 76,78,79,87–90,94,95,111–114,158,187–194,197–201,203–214,222–224,232,233,255–259]. In biological research, room temperature bioprinting of arrays of droplets made of bacteria, DNA, cells, various biopolymers, and proteins for gene expression studies and single-cell bioprinting for fundamental cellular biology are of high interest for the scientific community [204–206,225,255–259].

There are various methods of 3D bioprinting: droplet-based, extrusion-based, laser-based, and polymerization [69–76,78,79,204–214,225]. However, the high demand for precision, stretch ability, financial affordability, biocompatibility, reliability, and high-throughput fabrication of printed biological droplets strengthens the 3D droplet-based bioprinting [69–75,158,200,204–214,225].

Three-dimensional droplet-based bioprinting is an innovative and rapid technique to generate functional biological materials, such as cell laden 3D conformations for various clinical and healthcare applications [69]. The need for the 3D droplet-based bioprinting technique is supported by the numerous emerging medical application fields, including patient-specific artificial organs and tissues, regenerative medicine, high-throughput gene sequencing, pharmaceutical drug testing, 3D dental prostheses with specific architectures, 3D single-cell laden printing on stretchable and elastic materials, and physiological and pathological modeling [69–76,78,79,158,200,204–214,255–268].

It is extremely vital that the printed impacting biological droplet on a biocompatible material is perfectly isolated from other droplets to create a high bioprinting resolution

and precision [69,76,78,79,158,200,204–214,255–268]. Therefore, it is of great interest to gain deep insight on the physical mechanism and criteria that fully control the droplet spreading dynamics after impact and avoid any undesired splashing to maximize the bioprinting performance [69,76,78,79,158,200,204–214,225,255–268]. When spreading is not controllable in a process, barrier structures are often placed on the substrate via techniques such as lithography or stamping.

The essential requirement for 3D droplet-based bioprinting is to print biological ink droplets with detailed control to generate an error-free 3D pattern and shape of the biological sample on a biocompatible material. Thus, a detailed understanding of the physics of droplet spreading after impact on the material is crucial as it provides insights regarding 3D droplet-based bioprinting resolution and structural integrity and reliability [69,76,78,79,158,204–214,225,255–268].

2.2. Wearable/Portable/Implantable Biosensors

Wearable and portable biosensors have tremendous roles on numerous areas of personalized and precision medicine (Figure 2b,c) [58,59,69–72,195,234–245]. They can be used for the following: (1) medical diagnostic and monitoring on-chip devices; (2) medical diagnostic, monitoring, and therapeutic implants; (3) remote medical tracking systems; and (4) nanoscale-engineered smart and biocompatible medical materials.

More detailed examples of the personalized biomedical applications are as follows: (i) epidermal biosensors made of electrodes on flexible or stretchable substrates for energy harvesting and storage [315–319]; (ii) wearable integrated, real-time sweat monitoring biosensors that provide electrochemical swart information, such as lactate, uric acid, tyrosine, sodium, potassium, chloride, ammonia, glucose, and pH of the patient for the medical specialist [261,320–328]; and (iii) wearable biosensors that are applicable for monitoring tears and saliva of patients for healthcare and/or biomedical research to detect glucose and lactate [329–338].

The localization, tracking, and monitoring of smart ingestible biocompatible pills equipped with printed microdevices with nanobioelectronic ink droplets in the gastrointestinal tract are extremely precious for the diagnostics and treatment of gastrointestinal tract complications [58,59,69–76,234–245,255–268]. Such devices require high resolution and extremely controllable and precise nanoprinting of the active complex droplets in the wireless monitoring microdevice.

Considering the recent space race between countries, significant research started to participate in studies of human health during long-duration deep-space missions. Instantaneous and precise detection of stress and anxiety is crucial in human performance by controlling the mental health of the space passengers. Therefore, the development of wearable biosensors that have the potential of collecting physiological data such as deep-space stress and anxiety from the astronauts is extremely vital [195]. These advanced wearable biosensors are produced by printing biopolymer ink micro- or nanodroplets with electrical properties on flexible and biocompatible copolymer substrates.

One of the very popular areas of medical research is 3D-printed epifluidic electronic skin devices, which operate via the power of neural networks, for real-time health monitoring of each patient's physiological conditions, such as temperature, pulse, sweat, etc. [69]. These wearable sensors are produced by printing complex nanodroplets that are composed of various chemical components, such as numerous polymers, inorganic compounds, and numerous composites, on stretchable biocompatible substrates. These devices are equipped with a wireless electronic module, which is printed by nanoelectronic droplets, to remotely operate.

(**a**)

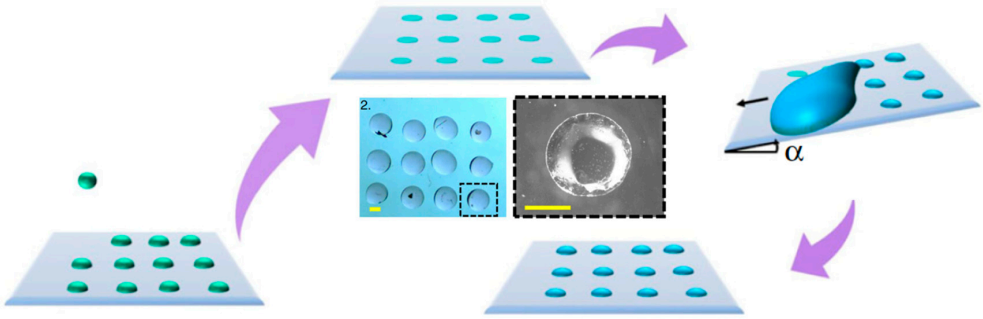

(**b**)

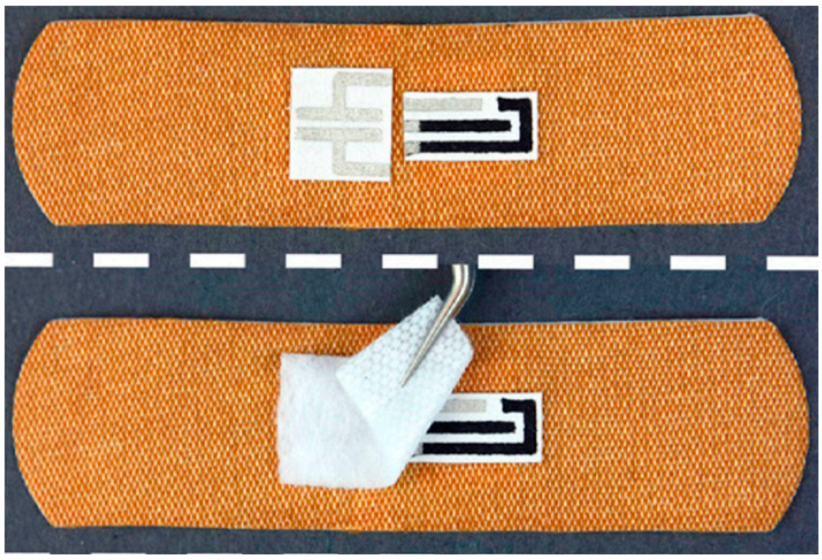

(**c**)

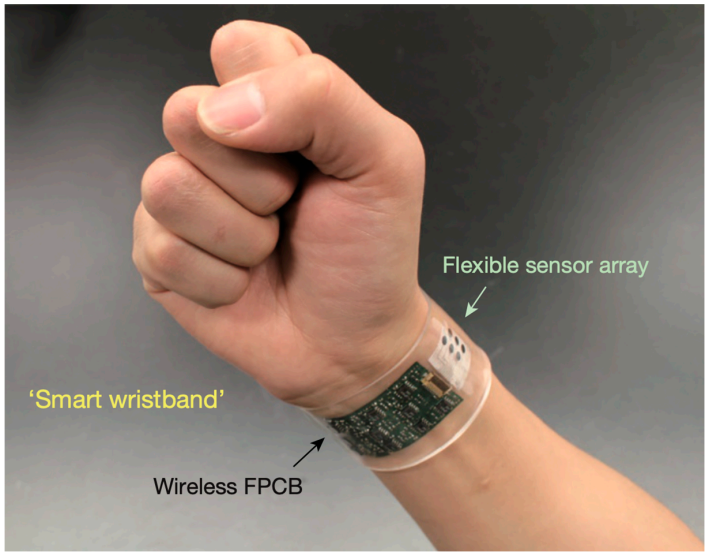

Figure 2. (**a**) State-of-the-art bioprinting technique based on the bioinspired droplet impact on various materials [225]. (**b**) Smart wireless wearable, flexible, integrated biosensing array on an individual's wrist for monitoring sweat data [319]. (**c**) Omniphobic paper-based smart bandages that monitor uric acid and pH level in the location of injury of the patient [261]. Reprinted from Nature Communications, 11, Modak, C. D., Kumar, A., Tripathy, A., and Sen, P. "Drop impact printing", 4327, Copyright (2020), with permission of Springer Nature. Reprinted from Biosensors and Bioelectronics,

117, Pal, A., Goswami, D., Cuellar, H.E., Castro, B., Kuang, S., Martinez, R.V. "Early detection and monitoring of chronic wounds using low-cost, omniphobic paper-based smart bandages", 696–705, Copyright (2018), with permission of Elsevier. Reprinted from Nature, 529, Gao, W., Emaminejad, S., Nyein, H.Y.Y., Challa, S., Chen, K., Peck, A., Fahad, H.M., Ota, H., Shiraki, H., Kiriya, D., Lien, D.H., Brooks, G.A., Davis, R.W., Javey, A. " Fully integrated wearable sensor arrays for multiplexed in situ perspiration analysis", 509–514, Copyright (2016), with permission of Springer Nature.

3. Droplet Motion on a Solid Surface

3.1. Contact Line

Once a droplet touches a solid surface, the contact line forms where the solid, liquid, and gas phases coexist (Figure 3a). After impact, the contact line moves on the solid surface. The level of contact line advancement on the solid surface is known as wettability. Wettability depends on the relative significance of the adhesive and the cohesive forces along the contact line [2,4,6,9,10,12,14,15,32,33,45,50,199,249,250]. The adhesive force promotes droplet advancement, whereas the cohesive forces resist the contact line motion. The physics of the moving contact line is important in various scientific fields, such as coatings, printings, microfluidics, energy, healthcare, and medicine [2,4,6,9,10,12,14,15,32,33,45,50,199,249,250, 255–268].

(**a**)

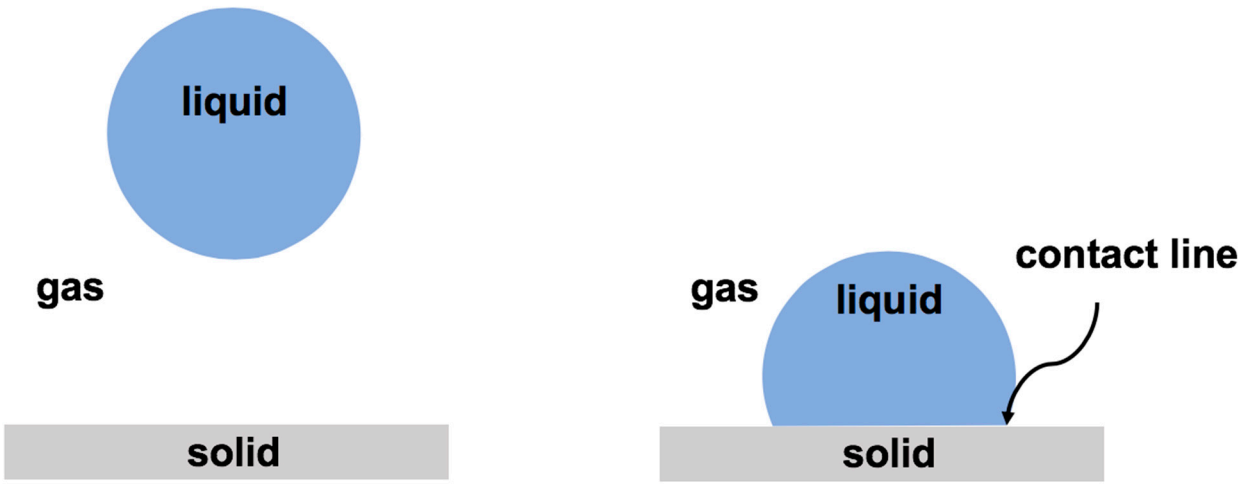

(**b**)

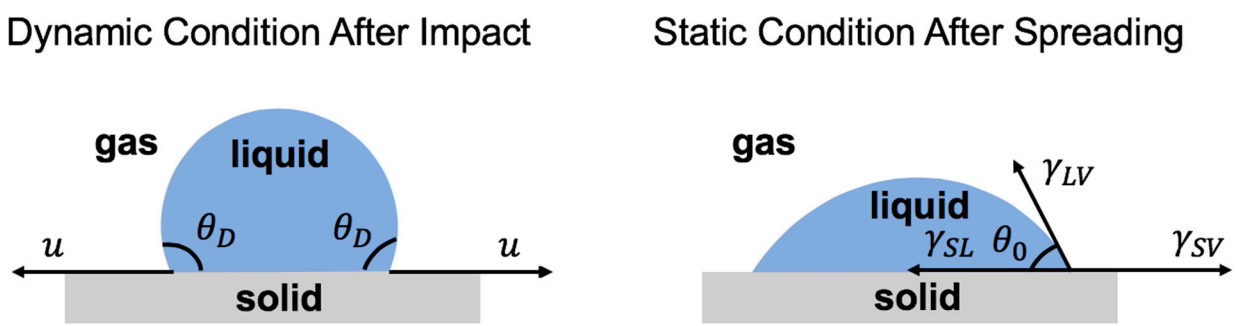

Figure 3. *Cont.*

(**c**)

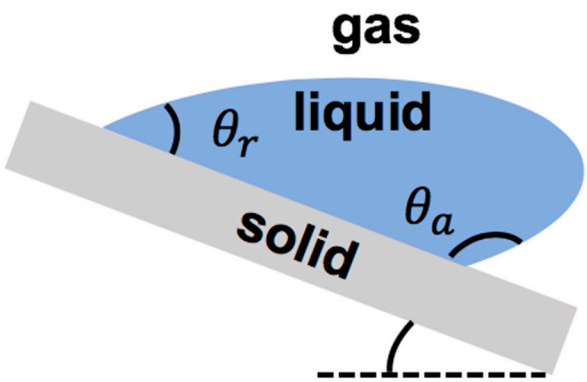

Figure 3. (**a**) Schematics of droplet falling onto a solid surface and forming a contact line. (**b**) Schematics of droplet on a solid surface during spreading (after impact) and at the equilibrium (after complete spreading). (**c**) Schematics of a moving droplet on an inclined surface with advancing and receding regions.

3.2. Contact Angle: Static and Dynamic

The dynamic contact angle (θ_D) is the angle between the liquid–air interface and the solid–liquid interface formed at the moving contact line [2,4,6,9,10,12,14,15,32,33,45,50]. Once the contact line becomes stationary, the contact angle reaches equilibrium and becomes static. The static contact angle (θ_0) is determined by Young's law, which is about the balance of the interfacial forces along the surface, as shown by Equation (1) [63]:

$$\gamma_{LV}\cos\theta_0 = (\gamma_{SV} - \gamma_{SL}) \tag{1}$$

in which γ_{LV} denotes the liquid–air surface tension, γ_{SV} presents the solid–air interfacial tension, and γ_{SL} is the solid–liquid interfacial tension (Figure 3b).

The static contact angle less than 90° represents a hydrophilic surface, the static contact angle between 90° and 150° presents a hydrophobic surface, and the static contact angle larger than 150° denotes a superhydrophobic surface. Depending on the direction of the motion of the moving contact line, such as droplet impact on an inclined surface, there are two types of contact angles: the advancing contact angle θ_a and the receding contact angle θ_r (Figure 3c). The difference between these two contact angles represents the contact angle hysteresis, which presents the geometric/chemical heterogeneity of the solid surface [35].

3.3. Contact Angle Modes: Wenzel, Cassie–Baxter, and Mixed

When a droplet impacts on a rough solid surface, one of the following theoretical models are valid: the Wenzel model and Cassie–Baxter model [160–162]. The Wenzel model states that the roughness on the solid surface increases the liquid–solid contact area by filling air pockets with liquid (Figure 4). Therefore, the contact angle in the Wenzel mode is determined by Equation (2):

$$\cos\theta_{Wenzel} = \chi\cos\theta_e \tag{2}$$

θ_{Wenzel} is the Wenzel static contact angle, and θ_e denotes the static contact angle on the horizontal smooth solid surface defined by Young's equation. χ presents the surface roughness, which signifies the ratio of the effective solid–liquid contact area to the projected droplet surface area on the rough surface ($\chi > 1$).

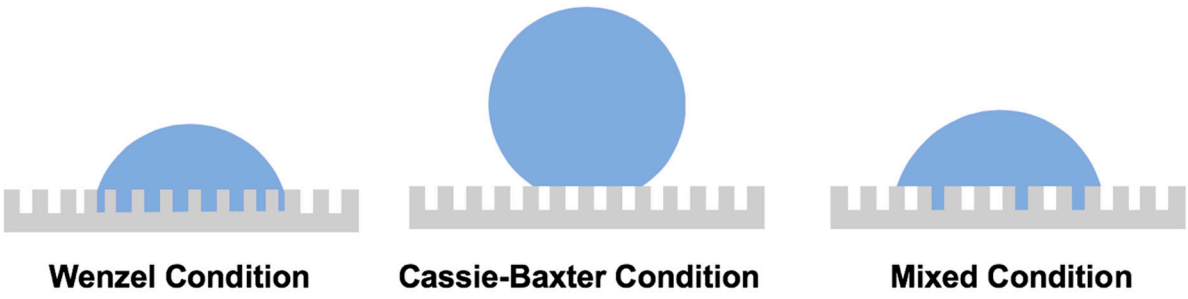

Figure 4. Schematics of droplet situation according to three physical models: Wenzel model, Cassie–Baxter model, and mixed model (i.e., combination of Wenzel and Cassie–Baxter models).

In the Cassie and Baxter mode, air pockets are presented between the droplet and the rough surface [161,162], as described by Equation (3) (Figure 4):

$$\cos\theta_{\text{Cassie}-\text{Baxter}} = \phi(\cos\theta_e + 1) - 1 \tag{3}$$

$\theta_{\text{Cassie}-\text{Baxter}}$ denotes the Cassie–Baxter static contact angle, and ϕ is the fraction of the solid surface in contact with the droplet. The Cassie–Baxter model is suitable for the droplet impact on a solid surface with chemical and/or geometric heterogeneity [68,69,72,133,163–196].

The existence of an alternative mixed mode has also been proposed in which part of the impacting droplet is in direct contact with the rough surface and its rest is held totally or partially on top of the air pockets (Figure 4) [197–199]. The mixed contact angle is defined by Equation (4):

$$\cos\theta_{\text{mixed_wetting}} = \chi\psi\cos\theta_e + \psi - 1 \tag{4}$$

in which ψ represents the percentage of the droplet-surface contact area.

3.4. Contact Line Dynamics

The dynamics of the moving contact line are defined by the complex relation between the dynamic contact angle (θ_D), the moving contact line velocity (u), the equilibrium receding contact angle (θ_{0r}), the equilibrium advancing contact angle (θ_{0a}), and several other physical parameters (δ): $F = f(\theta_D, u, \theta_{0a}, \theta_{0,r}, \delta)$ [3,7,8,23,33,39]. To explain the physics of the moving contact line, one must divide the vicinity of the contact line into three regions: macroscopic (outer region), mesoscopic (intermediate region), and microscopic (inner region), as illustrated in Figure 5 [2–4,6–10,12,14,15,23,32,33,39,45,50,113–115,117–119,199,249,250,255–268].

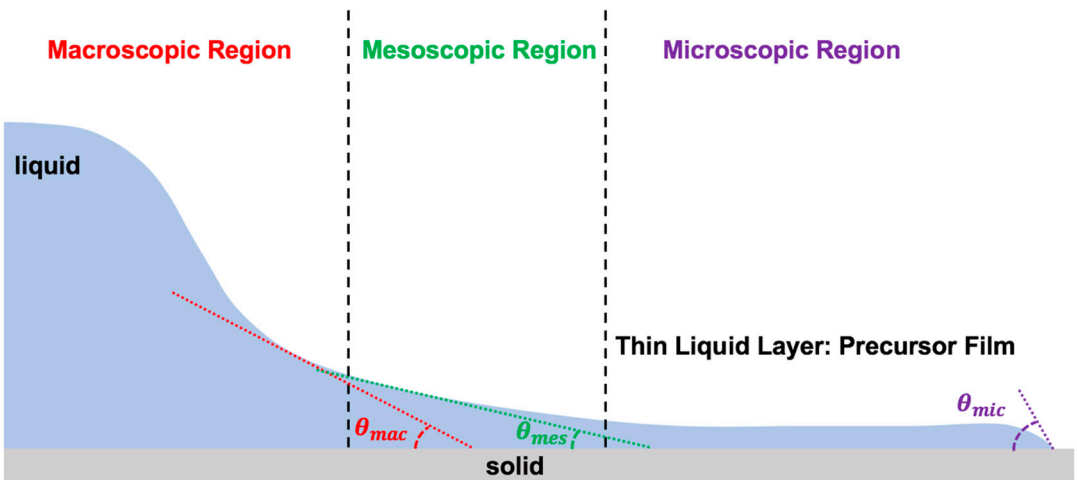

Figure 5. Three regions of the moving contact line with zoom in condition.

3.5. Physical Forces and Non-Dimensional Parameters

The physics of droplet impact on a solid surface is governed by three factors: the physical properties of the droplet and gaseous environment as well as the wettability of the solid surface. These factors can be defined by four physical forces: inertia, viscous, interfacial, and gravity [17,55–57,120,144,157,201,208,218,246–271]. Viscous force resists the droplet motion on the substrate through the viscous dissipation process. The interfacial tension denotes the droplet elasticity. The importance of gravity depends on the ratio of the droplet size and the capillary length ($\sqrt{\sigma/(\rho g)}$) in which ρ denotes droplet density, σ presents the surface tension, and g is the gravitational acceleration. Depending on the physical system, some external forces may be important to consider, such as the electric and magnetic fields and acoustic waves.

These physical forces can identify the physics of the droplet contact line after impact on a solid surface via the appropriate dimensionless parameters. These dimensionless parameters are the Reynolds number (Re), the Weber number (We), the Ohnesorge number (Oh), the capillary number (Ca), the Stokes number (St), the Bond number (Bo), the Froude number (Fr), the Weissenberg number (Wi), the Deborah number (De), and the elasto-capillary number (Ec) [17,68,69,253,254,272–279]. If any external force presents in the problem, additional dimensionless numbers can be introduced in the physics of the droplet contact line [8,11,17,33,54,68,69,104,105,253,254,272–279].

The Reynolds number is defined as the ratio of the inertia over the viscous force: $Re = \rho UD/\mu$. The Weber number describes the relative significance of inertia over the capillary force: $We = \rho U^2 D/\sigma$. The Ohnesorge number shows the balance between three physical forces (inertia, viscous force, and capillary force): $Oh = \mu/\sqrt{\rho\sigma D}$. The capillary number signifies the relative importance of viscous force over capillary force: $Ca = \mu U/\sigma$. The Stokes number is defined as the relative importance of gas viscosity (μ_g) over the inertia: $St = \mu_g/\rho UD$. The Bond number determines the relative effect of gravity over the capillary force: $Bo = \rho g D^2/\sigma$. The Froude number defines the ratio of the inertia over gravity: $Fr = U/\sqrt{gD}$. The Weissenberg number highlights the relative importance of elasticity over viscosity: $Wi = 2\dot{\gamma}\lambda$, where $\dot{\gamma}$ presents the shear rate of strain and λ denotes the relaxation time. The Deborah number defines the ratio of the relaxation time over characteristic time scale of the physical problem (t_c): $De = \lambda/t_c$. The elasto-capillary number defines the relative significance of $Ec = 2\dot{\gamma}\lambda\mu U/\sigma$. In these equations, which define the dimensionless numbers, μ is the droplet viscosity, ρ denotes the droplet density, D presents the droplet diameter, and U is the droplet contact line velocity. σ is the droplet surface tension.

The non-dimensional parameters are commonly used to categorize physical phenomena. The capillary length is used to distinguish between small and large droplets by providing physical meaning to small and large size in the droplet impact dynamics. The Reynolds number and Weber number are applied to verify the possibility of a splashing event in the droplet impact mechanism. The Bond number provides an insight to whether gravity is important in the physical situation. The Weissenberg number, Deborah number, and elasto-capillary number signify the viscoelasticity effect in the droplet impact physics.

3.6. Maximum Spreading Parameter

The maximum area over which the impacting droplet covers on a solid surface is denoted by a non-dimensional parameter known as the maximum spreading parameter (γ_{max}). The maximum spreading is defined as the maximum area that can be covered by the impacting droplet when the droplet reaches equilibrium on the solid surface and does not retract or leave the surface afterwards. The maximum spreading parameter has commonly been used to characterize the dynamics of the spreading of the impacting droplet [55–57,120,144,218,255–269]. The maximum spreading parameter is defined as the ratio of the droplet size at the end of spreading, D_s, over the initial droplet size, D_i.

Previous studies have attempted to formulate the maximum spreading parameter via other non-dimensional numbers. Laan et al. (2014) provided a list of the previous studies

in which they attempted to identify the maximum spreading parameter [75]. All these formulas were obtained based on theoretical analyses or experimental observations and by applying the three conservation laws: mass, momentum, and energy. They all concluded that the maximum spreading parameter depends on three non-dimensional parameters (i.e., Reynolds number, Weber number, and Ohnesorge number) as well as the Young static and dynamic contact angles. Furthermore, they found that these dependencies are in the power law: $\gamma_{max} \approx f\left(Re^l, We^m, Oh^n, \theta_0, \theta_D\right)$. It is important to note that, in all these studies, the droplet is assumed to not splash after impact on the solid surface. It is worth emphasizing that the calculated values of the maximum spreading parameter from all previous studies might differ from what is observed in the real physical situation. The formulas, which were obtained from all previous works, are only valid within certain limits and cannot be applied for complex droplets on real substrates.

It is important to mention that these findings only provide approximations for the maximum spreading parameter, since the level of accuracy is limited due to the limitation in observations caused by constraints in speed and resolution of imaging. Nevertheless, in healthcare and medicine, these formulas will not work as it is vital to have a high precision and accuracy to control the degree of spreading. Moreover, these findings are all applied for droplet impact on a rigid solid surface. In real applications, including healthcare and medicine, the solid is mostly flexible and heterogenous in terms of chemistry and geometry. Therefore, all these formulas need to be revisited by consideration of more practical surfaces and ultra-fast imaging techniques with very high resolutions in subangstrom, such as cryogenic electron microscopy. When high precision is required, one needs to add geometrical features on the substrate to control spreading. These features can be added by means of several techniques, including lithography or stamping [73].

4. Physical Models of Contact Line Dynamics

The physics of the moving contact line in various situations has been studied through a large number of theoretical, experimental, and numerical efforts [2–4,6–10,12,14,15,23,32,33,39,45,50,72,113–115,117–119,133,160–196,199,249,250,255–268]. The contact line dynamics involve the fluid dynamics and the interfacial physics [3,7,8,23,33,39]. The physics of the moving contact line has been commonly explained through the dependency of the dynamic contact angle to the contact line velocity along with the advancing and receding static contact angles [68,69,72,133,160–196]. There are six main physical models that conventionally explain the physics of the moving contact line: molecular kinetic (MK), hydrodynamics (HD), combined (MK–HD), precursor film, Shikhmurzaev, and Cahn–Hilliard–van der Waals.

4.1. Molecular Kinetic Model

Molecular kinetic theory explains the molecular dynamics at the vicinity of the dynamic contact in the microscopic region [3,114,115]. In molecular kinetic theory, it is postulated that liquid molecules in the microscopic region jump on the adsorption sites situated on the solid surface at the vicinity of the contact line (Figure 6). These molecular activities are controlled by the power of the energy barriers, which resist the contact line motion. In the molecular kinetic model, the physics of the moving contact line is formulated by the dependency of the contact line velocity to two molecular parameters, the frequency of the molecular dynamics (κ^0) and the distance between the adsorption sites (λ) at the contact line, as shown in Equation (5) [3,114,115]:

$$U = 2\kappa^0\lambda \sinh\left\{\frac{\pm\sigma\lambda^2[\cos\theta_0 - \cos\theta_D]}{2k_BT}\right\} \tag{5}$$

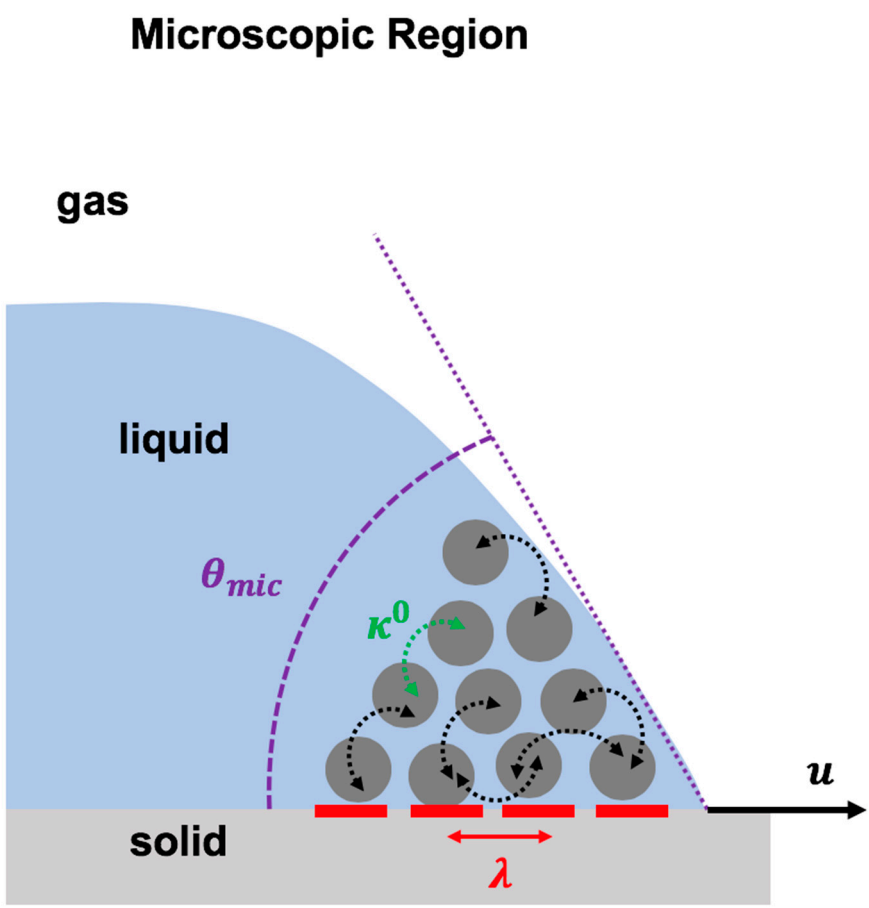

Figure 6. Schematic representation of the molecular kinetic theory to describe the physics of the moving contact line based on two molecular dynamic parameters: the frequency of molecular vibration in the microscopic region (κ^0) and the average distance between molecular adsorption sites on the solid surface (λ).

In Equation (5), k_B denotes the Boltzmann constant, and T represents the environment temperature with the unit in Kelvin.

As shown in Figure 6, λ presents the average distance between two adsorption sites that are located next to each other. These adsorption sites are the sites on the solid surface at which the liquid molecules attach or detach. κ^0 highlights the mean frequency of the molecular activity (molecular attachment/detachment on these adsorption sites) at the equilibrium condition.

4.2. Hydrodynamics Model

The hydrodynamics model explains the fluid dynamics near the moving contact line in the macroscopic region using Navier–Stokes equations for two-dimensional steady state flow based on lubrication assumption. Moreover, the hydrodynamics model applies the matched asymptotic expansions approach on the viscous bending of the liquid-free interface in the mesoscopic region of the flow (Figure 7). To resolve the issue of the violating boundary condition along the solid–liquid interface, at the moving contact line, it is assumed that the conventional no-slip boundary condition at the solid–liquid interface in the microscopic region must be relaxed over a distance known as the slip length (δ_s) [7,8,23,39,113,117–119].

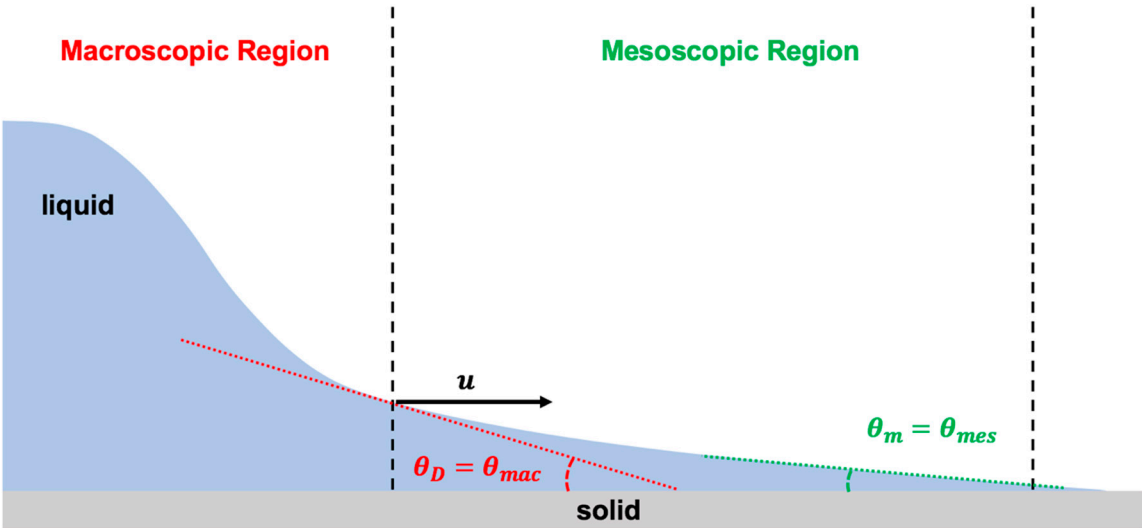

Figure 7. Schematic illustration of the physics of the moving contact line using hydrodynamics theory, which is based on bending of the liquid-free interface due to viscous effect at the vicinity of the moving contact line. Hydrodynamics theory considers two regions of the contact line: macroscopic (viscous bending) and mesoscopic (assumes Young static contact angle).

The conventional stress singularity at the moving contact line is relaxed within a distance called the slip length (δ_s), which is in the order of a few angstroms [4]. The slip length is related to the contact line speed and the liquid physical properties [4]. Accordingly, the slip length is defined by the capillary length (L_{cap}) and the capillary number (Ca): $\delta_s = L_{cap}Ca^{1/3}$ [4]. The capillary length shows the relative significance of the surface tension over gravity: $L_{cap} = \sqrt{\frac{\sigma}{\rho g}}$.

The hydrodynamics model depends on droplet size. For a large droplet (radius is larger than the capillary length), indeed there are two regions of interest in the contact line dynamics. However, for a small droplet, it is all about the mesoscopic region. Therefore, the hydrodynamics model determines the relation between the macroscopic dynamic contact angle (θ_D) to the capillary number (Ca) and the mesoscopic static contact angle (θ_m) in the inner region based on the viscous bending of the liquid-free interface in the mesoscopic region (Equations (6) and (7)) [7,8,23,39,113,117–119]:

$$\theta_D{}^3 - \theta_m{}^3 = \pm 9Ca\ln\left(\frac{L}{\delta_s}\right),\ \theta_D \leq \frac{3\pi}{4} \tag{6}$$

$$\frac{9\pi}{4}\ln\left\{\frac{1-\cos\theta_D}{1+\cos\theta_D}\right\} + (\pi-\theta_D)^3 - \theta_m{}^3 = \pm 9Ca\ln\left(\frac{L}{\delta_s}\right),\ \theta_D \geq \frac{3\pi}{4} \tag{7}$$

where L denotes the macroscopic characteristic length, δ_s presents the microscopic characteristic length (slip length), and the capillary number is the ratio of the viscous force over interfacial force: $Ca = \mu u/\sigma$ in which μ is the viscosity and σ is the surface tension.

4.3. Combined Model: Molecular Kinetic Model + Hydrodynamics Model

The combined model involves molecular kinetic theory and hydrodynamics theory to replace the constant mesoscopic static angle with the non-hydrodynamic variable static contact angle in the hydrodynamics model [3,114,181,293] as formulated in Equation (8):

$$\theta_D{}^3 - \left(\cos^{-1}\left[\cos\theta_0 \pm \left(\frac{2k_BT}{\sigma\lambda^2}\right)\sinh^{-1}\left(\frac{v}{2\kappa^0\lambda}\right)\right]\right)^3 = \pm 9Ca\ln\left(\frac{L}{\delta_s}\right) \tag{8}$$

The combined model claims that, by assigning a proper value for the three experimentally fitting parameters (κ^0, λ, δ_s), the physics of the contact line can be fairly estimated by the combination of the hydrodynamics and molecular kinetic theories [3,114,181].

The accuracy of the combined model strongly depends on the level of precision in the fitting analyses for determining the molecular kinetic and hydrodynamics parameters. There is a high possibility of overfitting, which leads to a significant weakness in its reliability. As a result, this model might not be a suitable model for applications that require strong precision and accuracy, such as healthcare, medicine, and biosensors.

4.4. Precursor Film Model

The physics of the dynamic contact line has been formulated by assuming the presence of a very thin layer of liquid well ahead of the contact line moving much faster than the apparent moving contact line [50,106,155] (Figure 8). The moving contact line dynamics were derived based on the precursor film by applying the absolute speed of molecular reactions based on molecular kinetic theory [60,106].

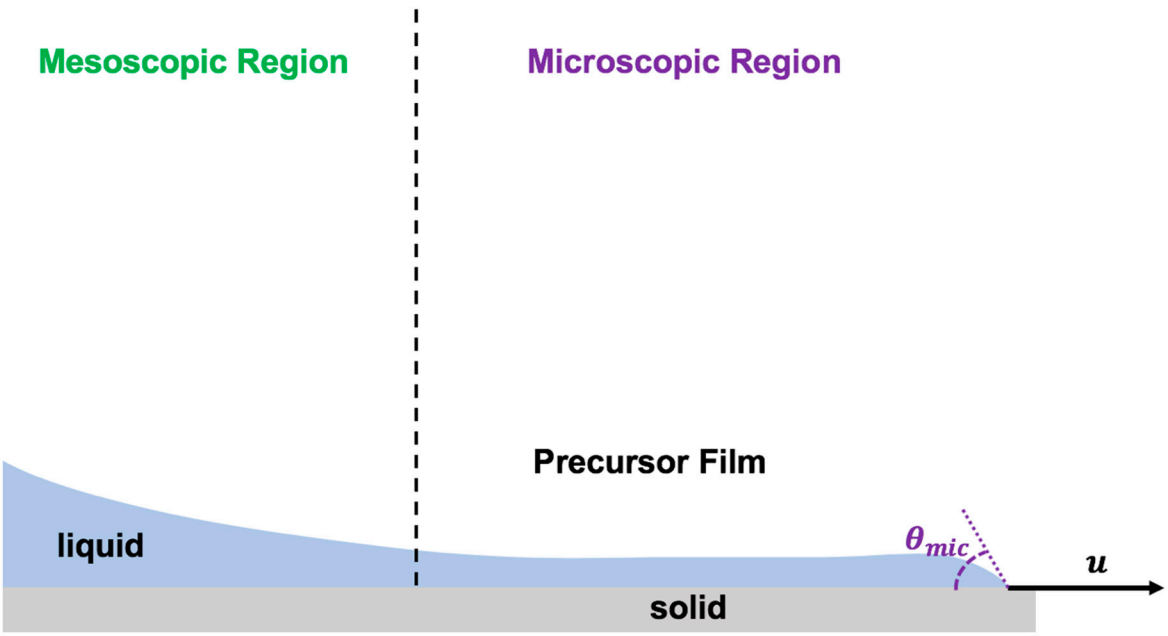

Figure 8. Schematics of the precursor film model to describe the physics of the moving contact line in the forefront of the advancing thin layer of droplet spreading.

In this model, the speed of the moving contact line was claimed to be driven by the sum of works done by van der Waals forces (W_{VDW}), polar molecular forces (W_{polar}), geometric forces ($W_{geometry}$), and any other type of forces, such as electric and/or magnetic forces (W_{other}). Therefore, the moving contact line velocity was formulated by Equation (9):

$$U = 2\kappa^0\lambda\sinh\left(\frac{\lambda^2\left(W_{VDW} + W_{polar} + W_{geometry} + W_{other}\right)}{2k_BT}\right) \quad (9)$$

It is important to note that the precursor film model requires very advanced computational tools with the help of supercomputers and state-of-the-art quantum computations to explain the physics of the moving contact line.

4.5. Shikhmurzaev Model

Shikhmurzaev considered the changes in interfacial tension forces in the microscopic region as the contact line moves on the solid surface and modeled the physics of the

moving contact line by applying the Navier–Stokes equations and the generalized Navier boundary conditions [269–271]. In the Shikhmurzaev model, the dynamic contact angle is postulated to be deviated from the classical Young static contact angle due to changes in the interfacial tensions from their equilibrium values at the static condition in the microscopic region [269–271]. The current Shikhmurzaev model is only applicable for smooth, chemically homogeneous solid surfaces.

4.6. Cahn–Hilliard–van der Waals Model

Cahn–Hilliard theory and van der Waals theory together explain the physics of the moving contact line via determining the dependency of the mesoscopic dynamic contact angle to the speed of the moving contact line [81–85,113]. In this model, the liquid–gas interface is an ultrathin layer (i.e., order of a few nanometer thickness) through which liquid properties vary significantly. They formulated their model by assuming the diffusion of the molecules across the interface. This model could resolve the long-standing challenging stress singularity boundary condition at the moving contact line, which was presented in the hydrodynamics model. This model can only be applied explicitly by powerful computational tools.

This model is suitable for liquids with multiple phases. Therefore, it has a promising potential application in healthcare and medicine in which the liquid droplets are composed of heterogeneous constituents, such as various proteins, hormones, enzymes, antibodies, etc. However, for its application on flexible biocompatible–biodegradable solid surfaces, it needs very serious modifications, as this model does not take into account the influence of the outer and inner regions on the dynamics of the moving contact line. The integral mechanical energy balance formula, derived from the generalized transport theorem as proposed by Slattery et al. 2007, could be the starting point to enhance the applicability of the Cahn–Hilliard–van der Waals model for biological droplet impact on biomaterials [74].

5. Future Directions

The printing of micro- and nanobiological droplets on wearable and biocompatible materials has been the center of attention in numerous modern technologies, such as smart biomaterials and advanced biosensors [200,225–232]. Droplets can contain biological samples and a suspension of micro- and nanosolid particles. In the bioprinting technique, it is extremely important for precise and controllable dispersion of micro- and nanodroplets on a solid surface. The state-of-the-art bioprinting approach can be applied for printing of numerous types of active complex biological droplets with desired sizes and components on biocompatible–wearable materials and elastic surfaces [200,225–229].

5.1. Future of Personalized Healthcare and Medicine by Wearable Biosensors

Promptly advancing research in personalized healthcare and medicine has shed light on the transformation of conventional healthcare and medicine. Wearable biosensors, which can monitor and control the physiological conditions of an individual and possibly treat lift-threatening diseases, present an extremely popular research topic for modern society.

Highly error-free biosensors with flexible and elastic biocompatible and biodegradable materials in healthcare demand extremely accurate formation of droplets that are composed of active biological macromolecules, such as proteins, enzymes, living cells, hormones, bacteria, viruses, and antibodies, onto the complex materials. Therefore, the previous findings for the maximum spreading parameter and the conventional theoretical–experimental–numerical approximations for simple liquids and solids are not appropriate for such highly demanding applications in healthcare and medicine.

It is important to expand the research in this field by utilizing multidisciplinary techniques covering various scientific disciplines, including biology, biochemistry, biophysics, interfacial physics, and electromagnetic physics, along with the use of state-of-the-art techniques, including deep neural networks, cryogenic electron microscopy, and quantum computing tools to harness the application of all aspects of the moving contact line

physics in all three regions of interest (macroscopic, mesoscopic, microscopic) as all regions equivalently contribute to the droplet motion for such complex systems.

Furthermore, it is extremely vital to simultaneously apply all physical models: molecular kinetic, hydrodynamics, precursor film, Shikhmurzaev, and Chan–Hilliard–van der Waals. Molecular kinetic describes activity in the microscopic region, hydrodynamics explains the macroscopic region with a connection with the mesoscopic zone, precursor film theory explicitly describes the molecular structure of the advanced microscopic region well ahead of the apparent contact line, Shikhmurzaev focuses on the changes in interfacial tensions due to activity of the molecules in the microscopic–mesoscopic zone, and Chan–Hilliard–van der Waals specifies the inter- and intra-molecular interactions via interface diffusion in the mesoscopic region. All three regions simultaneously interact with each other and subsequently influence the moving contact line for complex active biological droplets on an elaborate biocompatible–biodegradable solid surface.

Moreover, this highly demanding application becomes more complex when considering the application for personalized medicine. In personalized medicine, it is vital to consider all various physiological conditions of each specific individual. Therefore, the current physical models of the droplet moving contact line need to be revisited and modified to be applicable for complex physical situations in healthcare and medicine. Almost all these contact line dynamics models are explicitly suitable for simple conditions.

5.2. Nanodroplet Impact

Nanobioprinting is an innovative method for advancements in healthcare and medicine. In nanobioprinting, droplets with nanometer diameters are deposited on biocompatible materials. Consequently, it requires a considerably high level of precision and accuracy. This can be accomplished by controlling the contact line motion with high resolution on the surface. In nanobioprinting, it is vital to look deeply in the microscopic region and the influence of the mesoscopic region on the microscopic space. Therefore, connecting the multiple models of contact line dynamics is very crucial. Achievement of this goal needs ultra-fast imaging with extremely high resolution in sub-angstrom, such as the cryogenic electron microscope and the atomic force microscope. For validation of the experimental results, one needs to utilize high-performance computational tools and state-of-the-art neural networks and artificial intelligence on the large pool of data extracted from the experiments.

5.3. Physical Models of the Moving Contact Line: Limitations

Previous works that applied the energy equation reported approximate relations between the maximum spreading parameter and other non-dimensional parameters by only focusing on the mechanical energy. This is not a correct approach from energy conservation as the other forms of energy, including internal energy due to chemical/physical interactions between molecules, the thermal energy, as well as the entropy of the system, must be taken into account.

All current contact line models only look at the macroscopic region and/or mesoscopic region. This is not sufficient for applications in healthcare and medicine as they require high precision and accuracy in controlling the biological droplet contact line motion on an elastic stretchable biocompatible solid surface. Especially for nanobioprinting, tissue engineering, and artificial organs, it is extremely vital to look at the biological droplet contact line in nanoscale within the wide area of the microscopic region.

The current form of the molecular kinetic model is suitable to qualitatively describe the contact line dynamics. This limitation can be resolved by applying the power of neural networks and machine learning on the large pool of experimental observations obtained from the case of biological droplet impact dynamics to generate a quantitatively analytical formulation for the molecular kinetics parameters (κ^0 and λ).

The conventional hydrodynamics model is generally limited to the case of Newtonian solutions. The biological solutions are non-Newtonian. The hydrodynamics model needs to be revisited and modified to incorporate the role of non-Newtonian rheological charac-

teristics of the droplet in the model. This can be achieved by conducting experiments on impacting of biological droplets with various components, such as proteins, hormones, live cells, antibodies, live bacteria and viruses, etc., and taking advantage of the observations and state-of-the-art machine learning to revise the current model of hydrodynamics.

The credibility of the presence of an advancing thin layer ahead of the apparent moving contact line must be widely studied. The concept of precursor film is very critical for the case of bioprinting as it requires high precision and accuracy in nanoscale. The investigation in this area can be conducted by applying state-of-the-art nanotechnology and high-resolution imaging techniques, including atomic force microscopy and cryogenic electron microscopy.

Furthermore, almost all previous works only considered Newtonian or homogeneous droplets. In healthcare and medicine, droplets are non-Newtonian with active chemical/physical/biological interactions between biomacromolecules, such as living cells, bacteria, peptides, proteins, enzymes, and hormones, with very long complex molecular or self-assembled structures whose chemical and biophysical interactions with each other and the solid surface significantly influence the droplet contact line motion. These factors must be monitored by ultra-fast imaging techniques such as AFM with sub-angstrom resolution to resolve the chemical binding between biomacromolecules.

5.4. Evaporative Droplets

The contact line motion of evaporative biological droplets on biocompatible materials has significant interest in advanced biosensors for personalized healthcare. The coffee ring formation during the drying stage of the printed biological droplets could tremendously influence the reliability, precision, and accuracy of the bioprinting performance. The power of control on the dynamics of the moving contact line on such surfaces is extremely vital. Therefore, the volatility of the biological droplets must be taken into account and controlled during spreading. This can only be achieved by considering multiple physical models of the contact line that consider the influence of hydrodynamics in the macroscopic level on the drying events within the microscopic region. As a result, this requires the application of molecular kinetic, hydrodynamics, Chan–Hilliard–van der Waals, Shikhmurzaev, and, especially, precursor film. The inner region of the contact line, including the thin layer ahead of the apparent moving contact line, should be monitored using atomic force microscopy.

5.5. Heterogenous Biological Droplets

Biological droplets used in bioprinting and biosensors are commonly composed of numerous suspended biomacromolecules of different sizes, shapes, and chemical and physical properties. To provide high reliability, precision, and control of bioprinting techniques and biosensors, it is important to consider these factors during spreading of the impacting biological droplets. This challenge needs to be addressed by applying state-of-the-art technologies such as atomic force microscopy to monitor the contact line motion of such complex droplets and model the physics of such events by applying molecular kinetic, modified hydrodynamics, precursor film, Cahn–Hilliard–van der Waals, and Shikhmurzaev theories.

5.6. Future Perspective: Multi-Disciplinary Research

The innovative 3D bioprinting has the astonishing advantage to produce a wide range of functional biomaterials. This fascinating bioprinting technique can be utilized for numerous biomedical purposes, such as gene expression analysis, state-of-the-art stem cell research, artificial living organs, tissue engineering, advanced biosensors, and production of printed advanced biomaterials, which consist of living cells, DNA, bacteria, viruses, and proteins [200,225–229].

Considering the serious necessity for rapidly advancing bioprinting and biosensor technology, future research is expected to focus on applying the emerging technologies in electron microscopy, such as cryogenic electron microscopy, which is suitable for active

biological droplets, high-resolution atomic force microscopy, and a physics-informed data-driven approach for the science of droplet contact line dynamics after impact on materials (i.e., biocompatible, biodegradable, wearable) (Figure 9). It is important to apply all five current physical models of the moving contact line, as all three regions of the dynamic contact line need to be investigated for healthcare applications.

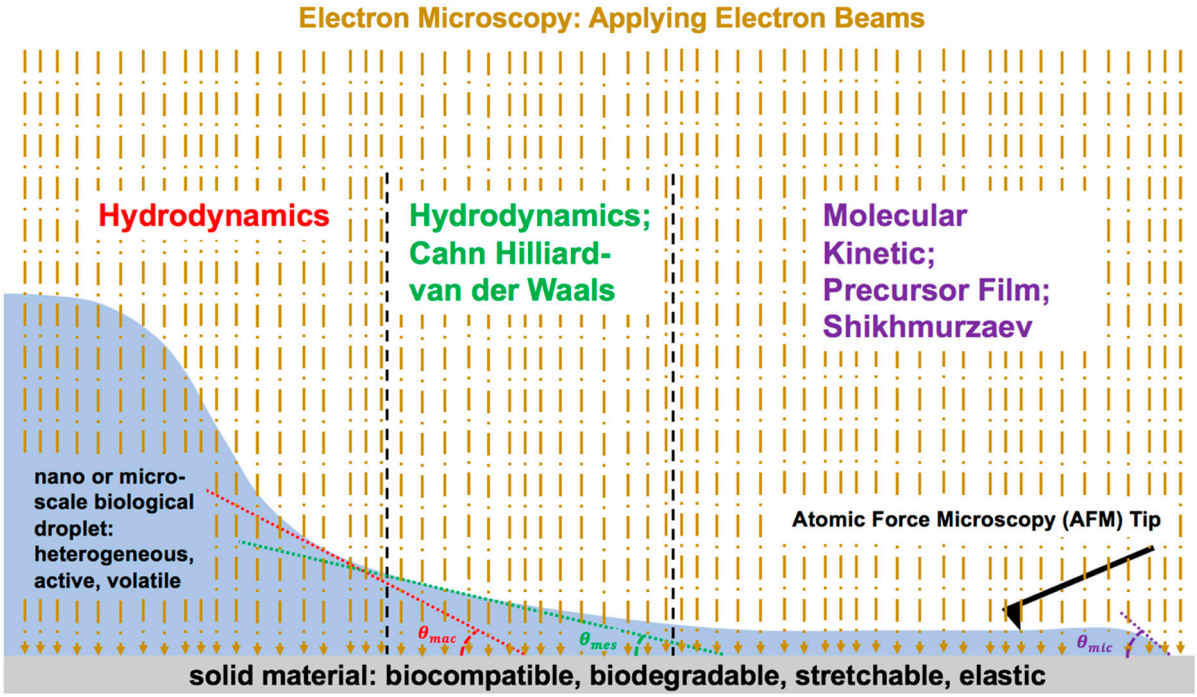

Figure 9. Schematic representation of future research direction: multi-disciplinary research combining nanotechnology, biology, materials science, and interfacial physics along with the combination of all physical models of the moving contact line in modified version.

Cell culture technique is a very common technique in biomedical research. In cell culture, the deposition of a precise amount of a cell-media droplet, such as human mitral valve interstitial cells diluted in full serum media on a collagen-coated plate for biomechanics studies of mitral valve diseases, is extremely critical for complete prevention of evaporation of the media on the cell culture plate and perfectly regulates the number of cells on the collagen-coated plate for gene analysis. Therefore, it is strongly vital to consider all theoretical models, including molecular kinetic theory, hydrodynamics theory, and precursor film, to evaluate the exact amount of live cell deposition on the collagen-coated plate via considering the evaporation of the precursor film of the cell-media solution droplet. These considerations have not yet been attempted.

This review article aims to highlight the drawbacks and limitations of the capabilities of the current physical models of droplet contact line dynamics upon impact in regard to its applicability and importance in biomedical research. The goal of this review article is to provide future road maps for research scientists in complex biological droplet impact upon a flexible plate and its contact line dynamics in various subjects of biomedicine and biomedical research, which have not been studied. The achievement of this goal requires revisiting the current physical models of the droplet liquid contact line upon impact on various solid surfaces. As of now, most works were experimental. The experimental data provide insights on the reality of each specific biophysical problem in the topic of the intersection of droplet impact dynamics and biomedicine. However, the experimental attempts do not provide a general thorough understanding of the various cases of biological droplet impact dynamics even for similar cases in biomedicine. Therefore, this review article emphasizes urgent advancements of the current versions of the physical models of

contact line dynamics of the biological droplets upon impact on solid plates by considering major revisions on all five physical models of the droplet contact line and combining them together to create a global physical model for droplet contact line dynamics to be applicable on the complex biofluid droplets in various topics of biomedical research.

Funding: This research received no external funding.

Data Availability Statement: There are no new data in this review article.

Conflicts of Interest: The author declares no conflict of interest.

References

1. Bird, J.C.; Dhiman, R.; Kwon, H.M.; Varanasi, K.K. Reducing the contact time of a bouncing drop. *Nature* **2013**, *503*, 385. [CrossRef] [PubMed]
2. Ren, W.; Weinan, E. Contact Line Dynamics on Heterogeneous Surfaces. *Phys. Fluids* **2011**, *23*, 072103. [CrossRef]
3. Blake, T.D. The Physics of Moving Wetting Lines. *J. Colloid Interface Sci.* **2006**, *299*, 1–13. [CrossRef] [PubMed]
4. Eggers, J.; Stone, H.A. Characteristic Lengths at Moving Contact Lines for a Perfectly Wetting Fluid: The Influence of Speed on The Dynamic Contact Angle. *J. Fluid Mech.* **2004**, *505*, 309–321. [CrossRef]
5. Yarin, A.L. Drop Impact Dynamics: Splashing, Spreading, Receding, Bouncing. *Annu. Rev. Fluid Mech.* **2006**, *38*, 159–192. [CrossRef]
6. Diaz, M.E.; Cerro, R.L. A General Solution of Dewetting Flow with a Moving Contact Line. *Phys. Fluids* **2021**, *33*, 103601. [CrossRef]
7. Cox, R.G. The Dynamics of the Spreading of Liquids on a Solid Surface. Part 1. Viscous Flow. *J. Fluid Mech.* **1986**, *168*, 169–194. [CrossRef]
8. Huh, C.; Scriven, J.L.E. Hydrodynamic Model of Steady Movement of a Solid/Liquid/Fluid Contact Line. *J. Colloid Interface Sci.* **1971**, *35*, 85–101. [CrossRef]
9. Harikrishnan, A.R.; Dhar, P.; Agnihotri, P.K.; Gedupudi, S.; Das, S.K. Correlating Contact Line Capillarity and Dynamic Contact Angle Hysteresis in Surfactant-Nanoparticle Based Complex Fluids. *Phys. Fluids* **2018**, *30*, 042006. [CrossRef]
10. Liu, M.; Chen, X.-P. Numerical Study on the Stick-Slip Motion of Contact Line Moving on Heterogeneous Surfaces. *Phys. Fluids* **2017**, *29*, 082102. [CrossRef]
11. Villermaux, E.; Bossa, B. Drop fragmentation on impact. *J. Fluid Mech.* **2011**, *668*, 412–435. [CrossRef]
12. Ding, H.; Spelt, P.D.M. Inertial Effects in Droplet Spreading: A Comparison between Diffuse-Interface and Level-Set Simulations. *J. Fluid Mech.* **2007**, *576*, 287–296. [CrossRef]
13. Kavehpour, H.P.; Mohammad Karim, A.; Rothstein, J.P.; Davis, S. Laws of Spreading: When Hydrodynamic Equations Are Not Enough. In Proceedings of the 70th Annual Meeting of the Fluid Dynamics, Denver, CO, USA, 19–21 November 2017; Division of the American Physical Society: College Park, MD, USA, 2017; Volume 62.
14. Biance, A.-L.; Clanet, C.; Quéré, D. First Steps in the Spreading of a Liquid Droplet. *Phys. Rev. E* **2004**, *69*, 016301. [CrossRef] [PubMed]
15. Foister, R.T. The Kinetics of Displacement Wetting in Liquid/Liquid/Solid Systems. *J. Colloid Interface Sci.* **1990**, *136*, 266–282. [CrossRef]
16. Marengo, M.; Antonini, C.; Roisman, I.V.; Tropea, C. Drop collisions with simple and complex surfaces. *Curr. Opin. Colloid Interface Sci.* **2011**, *16*, 292–302. [CrossRef]
17. Josserand, C.; Thoroddsen, S.T. Drop impact on a solid surface. *Annu. Rev. Fluid Mech.* **2016**, *48*, 365–391. [CrossRef]
18. Yarin, A.L.; Roisman, I.V.; Tropea, C. *Collision Phenomena in Liquids and Solids*; Cambridge University Press: Cambridge, UK, 2017.
19. Pierzyna, M.; Burzynski, D.A.; Bansmer, S.E.; Semaan, R. Data-driven splashing threshold model for drop impact on dry smooth surfaces. *Phys. Fluids* **2021**, *33*, 123317. [CrossRef]
20. Mohammad Karim, A.; Rothstein, J.P.; Kavehpour, H.P. Dynamics of Spreading on Micro-Textured Surfaces. In Proceedings of the 68th Annual Meeting of the Fluid Dynamics, Boston, MA, USA, 22–24 November 2015; Division of the American Physical Society: College Park, MD, USA, 2015; Volume 60.
21. Wijshoff, H. Drop dynamics in the inkjet printing process. *Curr. Opin. Colloid Interface Sci.* **2018**, *36*, 20–27. [CrossRef]
22. Mohammad Karim, A.; Rothstein, J.P.; Kavehpour, H.P. Experimental Study of Dynamic Contact Angles on Rough Hydrophobic Surfaces. *J. Colloid Interface Sci.* **2018**, *513*, 658–665. [CrossRef]
23. Voinov, O.V. Hydrodynamics of Wetting. *Fluid Dyn.* **1976**, *11*, 714–721. [CrossRef]
24. Mohammad Karim, A.; Kavehpour, H.P. Dynamics of Spreading on Ultra-hydrophobic Surfaces. *J. Coat. Technol. Res.* **2015**, *12*, 959–964. [CrossRef]
25. Wibowo, C.; Ng, K.M. Product-oriented process synthesis and development: Creams and pastes. *AIChE J.* **2001**, *47*, 2746–2767. [CrossRef]
26. Skurtys, O.; Aguilera, J.M. Applications of microfluidic devices in food engineering. *Food Biophys.* **2008**, *3*, 1–15. [CrossRef]
27. Singh, M.; Haverinen, H.M.; Dhagat, P.; Jabbour, G.E. Inkjet printing process and its applications. *Adv. Mater.* **2010**, *22*, 673–685. [CrossRef] [PubMed]

28. Zheng, B.; Roach, L.S.; Ismagilov, R.F. Screening of protein crystallization conditions on a microfluidic chip using nanoliter-size droplets. *J. Am. Chem. Soc.* **2003**, *125*, 11170–11171. [CrossRef]
29. Suea-Ngam, A.; Rattanarat, P.; Chailapakul, O.; Srisa-Art, M. Electrochemical droplet-based microfluidics using chip-based carbon paste electrodes for high-throughput analysis in pharmaceutical applications. *Anal. Chim. Acta* **2015**, *883*, 45–54. [CrossRef]
30. Mohammad Karim, A.; Suszynski, W.J.; Griffith, W.B.; Pujari, S.; Francis, L.F.; Carvalho, M.S. Effect of rheological properties of shear thinning liquids on curtain stability. *J. Non-Newton. Fluid Mech.* **2019**, *263*, 69–76. [CrossRef]
31. Singh, R.; Bahga, S.S.; Gupta, A. Electrohydrodynamic droplet formation in a T-junction microfluidic device. *J. Fluid Mech.* **2020**, *905*, A29. [CrossRef]
32. Spelt, P.D. A level-Set Approach for Simulations of Flows with Multiple Moving Contact Lines with Hysteresis. *J. Comput. Phys.* **2005**, *207*, 389–404. [CrossRef]
33. Wang, H. From Contact Line Structures to Wetting Dynamics. *Langmuir* **2019**, *35*, 10233–10245. [CrossRef]
34. Mohammad Karim, A.; Suszynski, W.J.; Pujari, S.; Francis, L.F.; Carvalho, M.S. Delaying Breakup and Avoiding Air Entrainment in Curtain Coating Using a Two-Layer Liquid Structure. *Chem. Eng. Sci.* **2020**, *213*, 115376. [CrossRef]
35. Brandon, S.; Marmur, A. Simulation of Contact Angle Hysteresis on Chemically Heterogeneous Surfaces. *J. Colloid Interface Sci.* **1996**, *183*, 351–355. [CrossRef] [PubMed]
36. Choi, K.; Ng, A.H.; Fobel, R.; Wheeler, A.R. Digital microfluidics. *Annu. Rev. Anal. Chem.* **2012**, *5*, 413–440. [CrossRef]
37. Mashaghi, S.; Abbaspourrad, A.; Weitz, D.A.; van Oijen, A.M. Droplet microfluidics: A tool for biology, chemistry and nanotechnology. *TrAC Trends Anal. Chem.* **2016**, *82*, 118–125. [CrossRef]
38. Mohammad Karim, A.; Suszynski, W.J.; Pujari, S.; Francis, L.F.; Carvalho, M.S. Stability of Two-Layer Curtain Coating. In Proceedings of the ICR 2020—18th International Congress on Rheology, Rio de Janeiro, Brazil, 2–7 August 2020.
39. De Gennes, P.G. Deposition of Langmuir-Blodgett Layers. *Colloid Polym. Sci.* **1986**, *264*, 463–465. [CrossRef]
40. Nguyen, N.-T.; Hejazian, M.; Ooi, C.; Kashaninejad, N. Recent advances and future perspectives on microfluidic liquid handling. *Micromachines* **2017**, *8*, 186. [CrossRef]
41. Song, H.; Chen, D.L.; Ismagilov, R.F. Reactions in droplets in microfluidic channels. *Angew. Chem. Int. Ed. Engl.* **2006**, *45*, 7336–7356. [CrossRef]
42. Teh, S.Y.; Lin, R.; Hung, L.H.; Lee, A.P. Droplet microfluidics. *Lab Chip* **2008**, *8*, 198–220. [CrossRef]
43. Weigl, B.H.; Bardell, R.L.; Cabrera, C.R. Lab-on-a-chip for drug development. *Adv. Drug Deliv. Rev.* **2003**, *55*, 349–377. [CrossRef]
44. Tao, X.; Chakrabarty, K. Parallel scan-like test and multiple-defect diagnosis for digital microfluidic biochips. *IEEE Trans. Biomed. Circuits Syst.* **2007**, *1*, 148–158.
45. Mohammad Karim, A.; Suszynski, W.J.; Pujari, S.; Francis, L.F.; Carvalho, M.S. Contact Line Dynamics in Curtain Coating of Non-Newtonian Liquids. *Phys. Fluids* **2021**, *33*, 103103. [CrossRef]
46. Mohammad Karim, A. Experimental Dynamics of Newtonian Non-elastic and Viscoelastic Droplets Impacting Immiscible Liquid Surface. *AIP Adv.* **2019**, *9*, 125141. [CrossRef]
47. Mohammad Karim, A. Experimental Dynamics of Newtonian and Non-Newtonian Droplets Impacting Liquid Surface with Different Rheology. *Phys. Fluids* **2020**, *32*, 043102. [CrossRef]
48. Joung, Y.S.; Buie, C.R. Aerosol generation by raindrop impact on soil. *Nat. Commun.* **2015**, *6*, 6083. [CrossRef]
49. Bourouiba, L. The fluid dynamics of disease transmission. *Annu. Rev. Fluid Mech.* **2021**, *53*, 473–508. [CrossRef]
50. Pham, T.; Kumar, S. Imbibition and Evaporation of Droplets of Colloidal Suspensions on Permeable Substrates. *Phys. Rev. Fluids* **2019**, *4*, 034004. [CrossRef]
51. Riboux, G.; Gordillo, J.M. Experiments of drops impacting a smooth solid surface: A model of the critical impact speed for drop splashing. *Phys. Rev. Lett.* **2014**, *113*, 024507. [CrossRef]
52. Xu, L.; Zhang, W.W.; Nagel, S.R. Drop splashing on a dry smooth surface. *Phys. Rev. Lett.* **2005**, *94*, 184505. [CrossRef]
53. Lee, M.; Chang, Y.S.; Kim, H.-Y. Drop impact on microwetting patterned surfaces. *Phys. Fluids* **2010**, *22*, 072101. [CrossRef]
54. Burzynski, D.A.; Roisman, I.V.; Bansmer, S.E. On the splashing of high-speed drops impacting a dry surface. *J. Fluid Mech.* **2020**, *892*, A2. [CrossRef]
55. Piskunov, M.; Semyonova, A.; Khomutov, N.; Ashikhmin, A.; Yanovsky, V. Effect of rheology and interfacial tension on spreading of emulsion drops impacting a solid surface. *Phys. Fluids* **2021**, *33*, 083309. [CrossRef]
56. Pasandideh-Fard, M.; Qiao, Y.M.; Chandra, S.; Mostaghimi, J. Capillary effects during droplet impact on a solid surface. *Phys. Fluids* **1996**, *8*, 650–659. [CrossRef]
57. Ukiwe, C.; Kwok, D. On the maximum spreading diameter of impacting droplets on well-prepared solid surfaces. *Langmuir* **2005**, *21*, 666–673. [CrossRef] [PubMed]
58. De la Paz, E.; Maganti, N.H.; Trifonov, A.; Jeerapan, I.; Mahato, K.; Yin, L.; Sonsa-Ard, T.; Ma, N.; Jung, W.; Burns, R.; et al. A self-powered ingestible wireless biosensing system for real-time in situ monitoring of gastrointestinal tract metabolites. *Nat. Commun.* **2022**, *13*, 7405. [CrossRef]
59. Sharma, S.; Ramadi, K.B.; Poole, N.H.; Srinivasan, S.S.; Ishida, K.; Kuosmanen, J.; Jenkins, J.; Aghlmand, F.; Swift, M.B.; Shapiro, M.G.; et al. Location-aware ingestible microdevices for wireless monitoring of gastrointestinal dynamics. *Nat. Electron.* **2023**, *6*, 242–256. [CrossRef]
60. Glasstone, S.; Laidler, K.J.; Eyring, H.J. *The Theory of Rate Processes*; McGraw-Hill: New York, NY, USA, 1941.

61. Jung, S.; Tiwari, M.K.; Doan, N.V.; Poulikakos, D. Mechanism of supercooled droplet freezing on surfaces. *Nat. Commun.* **2012**, *3*, 615. [CrossRef]
62. Mishchenko, L.; Hatton, B.; Bahadur, V.; Taylor, J.A.; Krupenkin, T.; Aizenberg, J. Design of ice-free nanostructured surfaces based on repulsion of impacting water droplets. *ACS Nano* **2010**, *4*, 7699–7707. [CrossRef]
63. Young, T. III. An essay on the cohesion of fluids. *Philos. Trans. R. Soc. Lond.* **1805**, *95*, 65–87. [CrossRef]
64. Chen, L.; Wu, J.; Li, Z.; Yao, S. Evolution of entrapped air under bouncing droplets on viscoelastic surfaces. *Colloids Surf. A Physicochem. Eng. Asp.* **2011**, *384*, 726–732. [CrossRef]
65. Blossey, R. Self-cleaning surfaces_virtual realities. *Nat. Mater.* **2003**, *2*, 301–306. [CrossRef]
66. Tuteja, A.; Choi, W.; Ma, M.; Mabry, J.M.; Mazzella, S.A.; Rutledge, G.C.; McKinley, G.H.; Cohen, R.E. Designing superoleophobic surfaces. *Science* **2007**, *318*, 1618–1622. [CrossRef]
67. Deng, X.; Mammen, L.; Butt, H.J.; Vollmer, D. Candle soot as a template for a transparent robust superamphiphobic coating. *Science* **2012**, *335*, 67–70. [CrossRef] [PubMed]
68. Chen, X.; ÓMahony, A.P.; Barber, T.J. Effect of 3D-bioprinted droplet impact dynamics on a pre-printed soft hydrogel matrix. *Exp. Fluids* **2023**, *64*, 60. [CrossRef]
69. Song, Y.; Tay, R.Y.; Li, J.; Xu, C.; Min, J.; Sani, E.S.; Kim, G.; Heng, W.; Kim, I.; Gao, W. 3D-printed epifluidic electronic skin for machine learning-powered multimodal health surveillance. *Sci. Adv.* **2023**, *9*, eadi6492. [CrossRef]
70. Yu, Y.; Li, J.; Solomon, S.A.; Min, J.; Tu, J.; Guo, W.; Xu, C.; Song, Y.; Gao, W. All-printed soft human-machine interface for robotic physicochemical sensing. *Sci. Robot.* **2022**, *7*, eabn0495. [CrossRef] [PubMed]
71. Bariya, M.; Shahpar, Z.; Park, H.; Sun, J.; Jung, Y.; Gao, W.; Nyein, H.Y.Y.; Liaw, T.S.; Tai, L.-C.; Ngo, Q.P.; et al. Roll-to-roll gravure printed electrochemical sensors for wearable and medical devices. *ACS Nano* **2018**, *12*, 6978–6987. [CrossRef] [PubMed]
72. Ota, H.; Chao, M.; Gao, Y.; Wu, E.; Tai, L.-C.; Chen, K.; Matsuoka, Y.; Iwai, K.; Fahad, H.M.; Gao, W.; et al. 3D printed earable smart devices for real-time detection of core body temperature. *ACS Sens.* **2017**, *2*, 990. [CrossRef]
73. Fang, A.; Dujardin, E.; Ondarçuhu, T. Control of droplet size in liquid nanodispensing. *Nano Lett.* **2006**, *6*, 2368–2374. [CrossRef]
74. Slattery, J.C.; Sagis, L.; Oh, E.S. *Interfacial Transport Phenomena*; Springer Science & Business Media: Berlin/Heidelberg, Germany, 2007.
75. Laan, N.; de Bruin, K.G.; Bartolo, D.; Josserand, C.; Bonn, D. Maximum diameter of impacting liquid droplets. *Phys. Rev. Appl.* **2014**, *2*, 044018. [CrossRef]
76. Yilmaz, B.; Al Rashid, A.; Mou, Y.A.; Evis, Z.; Koç, M. Bioprinting: A review of processes, materials and applications. *Bioprinting* **2021**, *23*, 00148. [CrossRef]
77. Yang, S.; Hou, Y.; Shang, Y.; Zhong, X. BPNN and CNN-based AI modeling of spreading and icing pattern of a water droplet impact on a supercooled surface. *AIP Adv.* **2022**, *12*, 045209. [CrossRef]
78. Ng, W.L.; Lee, J.M.; Zhou, M.; Chen, Y.W.; Lee, K.X.A.; Yeong, W.Y.; Shen, Y.F. Vat polymerization-based bioprinting-process, materials, applications and regulatory challenges. *Biofabrication* **2020**, *12*, 022001. [CrossRef] [PubMed]
79. Zhang, Y.; Kumar, P.; Lv, S.; Xiong, D.; Zhao, H.; Cai, Z.; Zhao, X. Recent advances in 3D bioprinting of vascularized tissues. *Mater. Des.* **2021**, *199*, 109398. [CrossRef]
80. Sun, L.; Pan, J.; Wang, X.; Jing, D. Molecular dynamics study of nanoscale droplets impacting on textured substrates of variable wettability. *Phys. Fluids* **2022**, *34*, 012005. [CrossRef]
81. Yue, P.; Zhou, C.; Feng, J.J. Sharp-Interface Limit of the Cahn–Hilliard Model for Moving Contact Lines. *J. Fluid Mech.* **2010**, *645*, 279–294. [CrossRef]
82. Yue, P.; Zhou, C.; Feng, J.J.; Ollivier-Gooch, C.F.; Hu, H.H. Phase-Field Simulations of Interfacial Dynamics in Viscoelastic Fluids Using Finite Elements with Adaptive Meshing. *J. Comput. Phys.* **2006**, *219*, 47–67. [CrossRef]
83. Van Der Waals, J.D. The Thermodynamic Theory of Capillarity Under the Hypothesis of a Continuous Variation of Density. *J. Stat. Phys.* **1979**, *20*, 200–244. [CrossRef]
84. Cahn, J.W. Critical Point Wetting. *J. Chem. Phys.* **1977**, *66*, 3667–3672. [CrossRef]
85. Cahn, J.W.; Hilliard, J.E. Free Energy of a Non-Uniform System. *Part I. Interfacial Free Energy. J. Chem. Phys.* **1958**, *28*, 258–267.
86. Quéré, D. Wetting and roughness. *Annu. Rev. Mater. Res.* **2008**, *38*, 71. [CrossRef]
87. Howland, C.J.; Antkowiak, A.; Castrejón-Pita, J.R.; Howison, S.D.; Oliver, J.M.; Style, R.W.; Castrejón-Pita, A.A. It's harder to splash on soft solids. *Phys. Rev. Lett.* **2016**, *117*, 184502. [CrossRef] [PubMed]
88. Ng, W.L.; Huang, X.; Shkolnikov, V.; Goh, G.L.; Suntornnond, R.; Yeong, W.Y. Controlling droplet impact velocity and droplet volume: Key factors to achieving high cell viability in sub-nanoliter droplet-based bioprinting. *Int. J. Bioprinting* **2022**, *8*, 424. [CrossRef] [PubMed]
89. Basso, B.C.; Bostwick, J.B. Splashing on soft elastic substrates. *Langmuir* **2020**, *36*, 15010–15017. [CrossRef] [PubMed]
90. Saile, D.; Kühl, V.; Gülhan, A. On the subsonic near-wake of a space launcher configuration without exhaust jet. *Exp. Fluids* **2019**, *60*, 50. [CrossRef]
91. Nilsson, M.A.; Rothstein, J.P. The effect of contact angle hysteresis on droplet coalescence and mixing. *J. Colloid Interface Sci.* **2011**, *363*, 646. [CrossRef]
92. Makrygianni, M.; Milionis, A.; Kryou, C.; Trantakis, I. On-demand laser printing of picoliter-sized, highly viscous, adhesive fluids: Beyond inkjet limitations. *Adv. Mater. Interfaces* **2018**, *5*, 1800440. [CrossRef]

93. Barthlott, W.; Neinhuis, C. Purity of the sacred lotus, or escape from contamination in biological surfaces. *Planta* **1997**, *202*, 1. [CrossRef]
94. Unagolla, J.M.; Jayasuriya, A.C. Hydrogel-based 3D bioprinting: A comprehensive review on cell-laden hydrogels, bioink formulations, and future perspectives. *Appl. Mater. Today* **2020**, *18*, 100479. [CrossRef]
95. Catros, S.; Guillotin, B.; Bačáková, M.; Fricain, J.-C.; Guillemot, F. Effect of laser energy, substrate film thickness and bioink viscosity on viability of endothelial cells printed by laser-assisted bioprinting. *Appl. Surf. Sci.* **2011**, *257*, 5142–5147. [CrossRef]
96. Ferraro, P.; Coppola, S.; Grilli, S.; Paturzo, M.; Vespini, V. Dispensing nano–pico droplets and liquid patterning by pyroelectrodynamic shooting. *Nat. Nanotechnol.* **2010**, *5*, 429. [CrossRef]
97. Srinivasan, S.; Choi, W.; Park, K.-C.; Chhatre, S.S.; Cohen, R.E.; McKinley, G.H. Drag reduction for viscous laminar flow on spray coated non-wetting surfaces. *Soft Matter* **2013**, *9*, 5691. [CrossRef]
98. Quéré, E. Non-sticking drops. *Rep. Prog. Phys.* **2005**, *68*, 2495. [CrossRef]
99. Rioboo, R.; Tropea, C.; Marengo, M. Outcomes from a drop impact on solid surfaces. *At. Sprays* **2001**, *11*, 155–165. [CrossRef]
100. Rein, M. Phenomena of liquid drop impact on solid and liquid surfaces. *Fluid Dyn. Res.* **1993**, *12*, 61. [CrossRef]
101. Li, J.; Rossignol, F.; Macdonald, J. Inkjet printing for biosensor fabrication: Combining chemistry and technology for advanced manufacturing. *Lab Chip* **2015**, *15*, 2538–2558. [CrossRef]
102. Bange, P.G.; Patil, N.D.; Bhardwaj, R. Impact Dynamics of a Droplet on a Heated Surface. In Proceedings of the 5th International Conference of Fluid Flow, Heat and Mass Transfer (FFHMT'18), Niagara Falls, ON, Canada, 7–9 June 2018; Volume 190, pp. 232–247.
103. Guo, Y.; Shen, S.; Yang, Y.; Liang, G.; Zhen, N. Rebound and spreading during a drop impact on wetted cylinders. *Exp. Therm. Fluid Sci.* **2013**, *52*, 97–103.
104. Malla, L.K.; Patil, N.D.; Bhardwaj, R.; Neild, A. Droplet bouncing and breakup during impact on a microgrooved surface. *Langmuir* **2017**, *33*, 9620–9631. [CrossRef]
105. Hamazaki, T.; Morita, N. Ejection characteristics and drop modulation of acoustic inkjet printing using fresnel lens. *J. Fluid Sci. Technol.* **2009**, *4*, 25–36. [CrossRef]
106. Derjaguin, B.; Churaev, N. Structural Component of Disjoining Pressure. *J. Colloid Interface Sci.* **1974**, *49*, 249–255. [CrossRef]
107. Andreotti, B.; Baumchen, O.; Boulogne, F.; Daniels, K.E.; Dufresne, E.R.; Perrin, H.; Salez, T.; Snoeijer, J.H.; Style, R.W. Solid capillarity: When and how does surface tension deform soft solids? *Soft Matter* **2016**, *12*, 2993. [CrossRef]
108. Boyer, F.; Sandoval-Nava, E.; Snoeijer, J.H.; Dijksman, J.F.; Lohse, D. Drop impact of shear thickening liquids. *Phys. Rev. Fluids* **2016**, *1*, 013901. [CrossRef]
109. Aytouna, M.; Bartolo, D.; Wegdam, G.; Bonn, D.; Rafaï, S. Impact dynamics of surfactant laden drops: Dynamic surface tension effects. *Exp. Fluids* **2010**, *48*, 49–57. [CrossRef]
110. Izbassarov, D.; Muradoglu, M. Effects of viscoelasticity on drop impact and spreading on a solid surface. *Phys. Rev. Fluids* **2016**, *1*, 023302. [CrossRef]
111. Utama, R.H.; Tan, V.T.G.; Tjandra, K.C.; Sexton, A.; Nguyen, D.H.T.; O'Mahony, A.P.; Du, E.Y.; Tian, P.; Ribeiro, J.C.C.; Kavallaris, M.; et al. A covalently crosslinked ink for multimaterials drop-on-demand 3D bioprinting of 3D cell cultures. *Macromol. Biosci.* **2021**, *21*, 2100125. [CrossRef] [PubMed]
112. Utama, R.H.; Atapattu, L.; O'Mahony, A.P.; Fife, C.M.; Baek, J.; Allard, T.; O'Mahony, K.J.; Ribeiro, J.; Gaus, K.; Kavallaris, M.; et al. Precise, high-throughput production of multicellular spheroids with a bespoke 3D bioprinter. *bioRxiv* **2020**. [CrossRef]
113. Dussan, V.E.B. On the Spreading of Liquids on Solid Surfaces: Static and Dynamic Contact Lines. *Annu. Rev. Fluid Mech.* **1979**, *11*, 371–400. [CrossRef]
114. Blake, T.D.; Berg, J.C. *Wettability: Dynamic Contact Angles and Wetting Kinetics*; Marcel Dekker: New York, NY, USA, 1993; Volume 49, pp. 251–309.
115. Blake, T.D.; Haynes, J.M. Kinetics of Liquid/Liquid Displacement. *J. Colloid Interf. Sci.* **1969**, *30*, 421–423. [CrossRef]
116. Wu, Z.; Cao, Y. Dynamics of initial drop splashing on a dry smooth surface. *PLoS ONE* **2017**, *12*, e0177390. [CrossRef]
117. Huh, C.; Mason, S.G. The Steady Movement of a Liquid Meniscus in a Capillary Tube. *J. Fluid Mech.* **1977**, *81*, 401–419. [CrossRef]
118. Dussan, V.E.B. The Moving Contact Line: The Slip Boundary Condition. *J. Fluid Mech.* **1976**, *77*, 665–684. [CrossRef]
119. Ngan, C.G.; Dussan, V.E.B. On the Dynamics of Liquid Spreading on Solid Surfaces. *J. Fluid Mech.* **1989**, *209*, 191–226. [CrossRef]
120. Schroll, R.D.; Josserand, C.; Zaleski, S.; Zhang, W.W. Impact of a viscous liquid drop. *Phys. Rev. Lett.* **2010**, *104*, 034504. [CrossRef] [PubMed]
121. Coppola, G.; Rocco, G.; de Luca, L. Insights on the impact of a plane drop on a thin liquid film. *Phys. Fluids* **2011**, *23*, 022105. [CrossRef]
122. Josserand, C.; Ray, P.; Zaleski, S. Droplet impact on a thin liquid film: Anatomy of the splash. *arXiv* **2015**, *1511*, 09395. [CrossRef]
123. Mahady, K.; Afkhami, S.; Kondic, L. A volume of fluid method for simulating fluid/fluid interfaces in contact with solid boundaries. *J. Comput. Phys.* **2015**, *294*, 243–257. [CrossRef]
124. Couder, Y.; Protière, S.; Fort, E.; Boudaoud, A. Walking and orbiting droplets. *Nature* **2005**, *437*, 208. [CrossRef]
125. Couder, Y.; Fort, E.; Gautier, C.-H.; Boudaoud, A. From bouncing to floating: Nanocoalescence of drops on a fluid bath. *Phys. Rev. Lett.* **2005**, *94*, 177801. [CrossRef]
126. Lee, A.; Jin, H.; Dang, H.-W.; Choi, K.-H.; Ahn, K.H. Optimization of experimental parameters to determine the jetting regimes in electrohydrodynamic printing. *Langmuir* **2013**, *29*, 13630–13639. [CrossRef]

127. Šikalo, Š.; Wilhelm, H.-D.; Roisman, I.V.; Jakirlić, S.; Tropea, C. Dynamic contact angle of spreading droplets: Experiments and simulations. *Phys. Fluids* **2005**, *17*, 062103. [CrossRef]
128. Gunjal, P.R.; Ranade, V.V.; Chaudhari, R.V. Dynamics of drop impact on solid surface: Experiments and VOF simulations. *AIChE J.* **2005**, *51*, 59–78. [CrossRef]
129. Sahoo, N.; Khurana, G.; Harikrishnan, A.R.; Samanta, D.; Dhar, P. Post impact droplet hydrodynamics on inclined planes of variant wettabilities. *Eur. J. Mech. B Fluids* **2020**, *79*, 27–37. [CrossRef]
130. Shang, Y.; Zhang, Y.; Hou, Y.; Bai, B.; Zhong, X. Effects of surface subcooling on the spreading dynamics of an impact water droplet. *Phys. Fluids* **2020**, *32*, 123309. [CrossRef]
131. Cui, Z.; Wang, W.; Guo, L.; Liu, Z.; Cai, P.; Cui, Y.; Wang, T.; Wang, C.; Zhu, M.; Zhou, Y.; et al. Haptically quantifying Young's modulus of soft materials using a self-locked stretchable strain sensor. *Adv. Mater.* **2021**, *34*, 2104078. [CrossRef] [PubMed]
132. Mohammad Karim, A.; Davis, S.H.; Kavehpour, H.P. Forced versus Spontaneous Spreading of Liquids. *Langmuir* **2016**, *32*, 10153–10158. [CrossRef] [PubMed]
133. Mohammad Karim, A.; Suszynski, W.J.; Francis, L.F.; Carvalho, M.S. Effect of Viscosity on Liquid Curtain Stability. *AIChE J.* **2018**, *64*, 1448–1457. [CrossRef]
134. Mohammad Karim, A.; Kavehpour, H.P. Effect of Viscous Force on Dynamic Contact Angle Measurement Using Wilhelmy Plate Method. *Colloids Surf. A* **2018**, *548*, 54–60. [CrossRef]
135. Li, E.Q.; Thoroddsen, S.T. Time-resolved imaging of a compressible air-disc under a drop impacting on a solid surface. *J. Fluid Mech.* **2015**, *780*, 636–648. [CrossRef]
136. Driscoll, M.M.; Stevens, C.S.; Nagel, S.R. Thin film formation during splashing of viscous liquids. *Phys. Rev. E* **2010**, *83*, 036302. [CrossRef]
137. Thoroddsen, S.T.; Takehara, K.; Etoh, T.G. Micro-splashing by drop impacts. *J. Fluid Mech.* **2012**, *706*, 560–570. [CrossRef]
138. Thoroddsen, S.T.; Sakakibara, J. Evolution of the fingering pattern of an impacting drop. *Phys. Fluids* **1998**, *10*, 1359–1374. [CrossRef]
139. Bischofberger, I.; Mauser, K.W.; Nagel, S.R. Seeing the invisible-air vortices around a splashing drop. *Phys. Fluids* **2013**, *25*, 091110. [CrossRef]
140. Abouelsoud, M.; Bai, B. Bouncing and coalescence dynamics during the impact of a falling drop with a sessile drop on different solid surfaces. *Phys. Fluids* **2021**, *33*, 063309. [CrossRef]
141. Dalgamoni, H.N.; Yong, X. Numerical and theoretical modeling of droplet impact on spherical surfaces. *Phys. Fluids* **2021**, *33*, 052112. [CrossRef]
142. Zhou, J.; Wang, X.; Su, J.; Jing, D.; Mohamad, A.A. Impact on mechanical robustness of water droplet due to hydrophilic nanoparticles. *Phys. Fluids* **2020**, *32*, 122110. [CrossRef]
143. Yee, J.; Yamanaka, A.; Tagawa, Y. Image features of a splashing drop on a solid surface extracted using a feedforward neural network. *Phys. Fluids* **2022**, *34*, 013317. [CrossRef]
144. Vadillo, D.; Soucemarianadin, A.; Delattre, C.; Roux, D. Dynamic contact angle effects onto the maximum drop impact spreading on solid surfaces. *Phys. Fluids* **2009**, *21*, 122002. [CrossRef]
145. Mongruel, A.; Daru, V.; Feuillebois, F.; Tabakova, S. Early post-impact time dynamics of viscous drops onto a solid dry surface. *Phys. Fluids* **2009**, *21*, 032101. [CrossRef]
146. Stevens, C.S.; Latka, A.; Nagel, S.R. Comparison of splashing in high- and low-viscosity liquids. *Phys. Rev. E* **2014**, *89*, 063006. [CrossRef]
147. Liu, Y.; Tan, P.; Xu, L. Kelvin-Helmholtz instability in an ultrathin air film causes drop splashing on smooth surfaces. *Proc. Natl. Acad. Sci. USA* **2015**, *112*, 3280–3284. [CrossRef]
148. Mishra, N.K.; Zhang, Y.; Ratner, A. Effect of chamber pressure on spreading and splashing of liquid drops upon impact on a dry smooth stationary surface. *Exp. Fluids* **2011**, *51*, 483–491. [CrossRef]
149. Fabmann, B.W.; Bansmer, S.E.; Möller, T.J.; Radespiel, R.; Hartmann, M. High velocity impingement of single droplets on a dry smooth surface. *Exp. Fluids* **2013**, *54*, 1516.
150. Palacios, J.; Hernández, J.; Gómez, P.; Zanzi, C.; López, J. On the impact of viscous drops onto dry smooth surfaces. *Exp. Fluids* **2012**, *52*, 1449–1463. [CrossRef]
151. Kittel, H.M.; Roisman, I.V.; Tropea, C. Splash of a drop impacting onto a solid substrate wetted by a thin film of another liquid. *Phys. Rev. Fluids* **2018**, *3*, 073601. [CrossRef]
152. Reiser, A.; Lindén, M.; Rohner, P.; Marchand, A.; Galinski, H.; Sologubenko, A.S.; Wheeler, J.M.; Zenobi, R.; Poulikakos, D. Multi-metal electrohydrodynamic redox 3D printing at the submicron scale. *Nat. Commun.* **2019**, *10*, 1853. [CrossRef]
153. Mohammad Karim, A.; Kim, J.; Rothstein, J.P.; Kavehpour, H.P. Dynamics of Wetting of Ultra-hydrophobic Surfaces. In Proceedings of the 66th Annual Meeting of the Fluid Dynamics, Pittsburgh, PA, USA, 24–26 November 2013; Division of the American Physical Society: College Park, MD, USA, 2013; Volume 58.
154. Mohammad Karim, A.; Kavehpour, H.P. Spreading of Emulsions on Glass Substrates. In Proceedings of the 65th Annual Meeting of the Fluid Dynamics, San Diego, CA, USA, 18–20 November 2012; Division of the American Physical Society: College Park, MD, USA, 2012; Volume 57.
155. Yuan, Q.; Zhao, Y.-P. Precursor Film in Dynamic Wetting, Electrowetting, and Electro-Elasto-Capillarity. *Phys. Rev. Lett.* **2010**, *104*, 246101. [CrossRef]

156. Mohammad Karim, A.; Kavehpour, H.P. Laws of spreading: Why Tanner, Hoffman, Voinov, Cox and de Gennes were wrong, generally speaking. In Proceedings of the 67th Annual Meeting of the Fluid Dynamics, San Francisco, CA, USA, 23–25 November 2014; Division of the American Physical Society: College Park, MD, USA, 2014; Volume 59.
157. Mohammad Karim, A.; Kavehpour, H.P. Spreading of Emulsions on a Solid Substrate. *J. Coat. Technol. Res.* **2014**, *11*, 103–108. [CrossRef]
158. Vanaei, S.; Parizi, M.S.; Vanaei, S.; Salemizadehparizi, F.; Vanaei, H.R. An overview on materials and techniques in 3D bioprinting toward biomedical application. *Eng. Regen.* **2021**, *2*, 1–18. [CrossRef]
159. Rao, D.N. The concept, characterization, concerns and consequences of contact angles in solid-liquid-liquid systems. In Proceedings of the 3rd International Symposium on Contact Angle, Wettability and Adhesion, Providence, RI, USA, 20–23 May 2002; Volume 3, pp. 191–210.
160. Wenzel, R.N. Resistance of solid surfaces to wetting by water. *Ind. Eng. Chem.* **1936**, *28*, 988–994. [CrossRef]
161. Cassie, A.B.D.; Baxter, S. Wettability of porous surfaces. *Trans. Faraday Soc.* **1944**, *40*, 546–551. [CrossRef]
162. Cassie, A.B.D. Contact angles. *Discuss Faraday Soc.* **1948**, *3*, 11–16. [CrossRef]
163. Israelachvili, J.N.; Gee, M.L. Contact angles on chemically heterogeneous surfaces. *Langmuir* **1989**, *5*, 288–289. [CrossRef]
164. Gao, L.C.; McCarthy, T.J. How Wenzel and Cassie were wrong? *Langmuir* **2007**, *23*, 3762–3765. [CrossRef] [PubMed]
165. Larsen, S.T.; Taboryski, R.A. Cassie-like law using triple phase boundary line fractions for faceted droplets on chemically heterogeneous surfaces. *Langmuir* **2009**, *25*, 1282–1284. [CrossRef] [PubMed]
166. Choi, W.; Tuteja, A.; Mabry, J.M.; Cohen, R.E.; McKinley, G.H. A modified Cassie-Baxter relationship to explain contact angle hysteresis and anisotropy on non-wetting textured surfaces. *J. Colloid Interface Sci.* **2009**, *339*, 208–216. [CrossRef] [PubMed]
167. Milne, A.J.B.; Amirfazli, A. The Cassie equation: How it is meant to be used. *Adv. Colloid Interface Sci.* **2012**, *170*, 48–55. [CrossRef]
168. Mohammad Karim, A.; Suszynski, W.J.; Griffith, W.B.; Pujari, S.; Francis, L.F.; Carvalho, M.S. Effect of Viscoelasticity on Stability of Liquid Curtain. *J. Non-Newton. Fluid Mech.* **2018**, *257*, 83–94. [CrossRef]
169. Wang, X.; Xu, B.; Chen, Z.; Yang, Y.; Cao, Q. Effects of gravitational force and surface orientation on the jumping velocity and energy conversion efficiency of coalesced droplets. *Microgravity Sci. Tec.* **2020**, *32*, 1185–1197. [CrossRef]
170. Hail, C.U.; Höller, C.; Matsuzaki, K.; Rohner, P.; Renger, J.; Sandoghdar, V.; Poulikakos, D.; Eghlidi, H. Nanoprinting organic molecules at the quantum level. *Nat. Commun.* **2019**, *10*, 1880. [CrossRef]
171. Eggers, J.; Lister, J.R.; Stone, H.A. Coalescence of liquid drops. *J. Fluid Mech.* **1999**, *401*, 293–310. [CrossRef]
172. Joseph, D.P.; Justin, C.B.; Sidney, R.N.; Santosh, A.; Michael, T.H.; Osman, A.B. The inexorable resistance of inertia determines the initial regime of drop coalescence. *Proc. Natl. Acad. Sci. USA* **2012**, *109*, 6857–6861.
173. Wang, X.Y.; Jia, L. Experimental study on heat transfer performance of pulsating heat pipe with refrigerants. *J. Therm. Sci.* **2016**, *25*, 449–453. [CrossRef]
174. Wiedenheft, K.F.; Guo, H.A.; Qu, X.P.; Boreyko, J.B.; Liu, F.J.; Zhang, K.G.; Eid, F.; Choudhury, A.; Li, Z.H.; Chen, C.H. Hotspot cooling with jumping-drop vapor chambers. *Appl. Phys. Lett.* **2017**, *110*, 141601. [CrossRef]
175. McNeil, D.A.; Burnside, B.M.; Cuthbertson, G. Dropwise condensation of steam on a small tube bundle at turbine condenser conditions. *Exp. Heat Transf.* **2000**, *13*, 89–105.
176. Song, K.; Kim, G.; Oh, S.; Lim, H. Enhanced water collection through a periodic array of tiny holes in dropwise condensation. *Appl. Phys. Lett.* **2018**, *112*, 071602. [CrossRef]
177. Humplik, T.; Lee, J.; O'Hern, S.C.; Fellman, B.A.; Baig, M.A.; Hassan, S.F.; Atieh, M.A.; Rahman, F.; Laoui, T.; Karnik, R.; et al. Nanostructured materials for water desalination. *Nanotechnology* **2011**, *22*, 292001. [CrossRef] [PubMed]
178. Delrot, P.; Modestino, M.A.; Gallaire, F.; Psaltis, D.; Moser, C. Inkjet printing of viscous monodisperse microdroplets by laser-induced flow focusing. *Phys. Rev. Appl.* **2016**, *6*, 24003. [CrossRef]
179. Min, J.; Sempionatto, J.R.; Teymourian, H.; Wang, J.; Gao, W. Wearable electrochemical biosensors in North America. *Biosens. Bioelectron.* **2021**, *172*, 112750. [CrossRef]
180. Ju, J.; Bai, H.; Zheng, Y.; Zhao, T.; Fang, R.; Jiang, L. A multi-structural and multi-functional integrated fog collection system in cactus. *Nat. Commun.* **2012**, *3*, 1247. [CrossRef]
181. Petrov, P.G.; Petrov, J.G. A Combined Molecular-Hydrodynamic Approach to Wetting Kinetics. *Langmuir* **1992**, *8*, 1762–1767. [CrossRef]
182. Ghosh, A.; Beaini, S.; Zhang, B.J.; Ganguly, R.; Megaridis, C.M. Enhancing dropwise condensation through bioinspired wettability patterning. *Langmuir* **2014**, *30*, 13103–13115. [CrossRef]
183. Parker, A.R.; Lawrence, C.R. Water capture by a desert beetle. *Nature* **2001**, *414*, 33–34. [CrossRef] [PubMed]
184. Feng, S.; Delannoy, J.; Malod, A.; Zheng, H.; Quéré, D.; Wang, Z. Tip-induced flipping of droplets on Janus pillars: From local reconfiguration to global transport. *Sci. Adv.* **2020**, *6*, eabb4540. [CrossRef] [PubMed]
185. Hou, Y.; Yu, M.; Chen, X.; Wang, Z.; Yao, S. Recurrent filmwise and dropwise condensation on a beetle mimetic surface. *ACS Nano* **2015**, *9*, 71–81. [CrossRef] [PubMed]
186. Wang, Y.; Feng, Z.; Frechette, J. Dynamic adhesion due to fluid infusion. *Curr. Opin. Colloid Interface Sci.* **2020**, *50*, 101397. [CrossRef]
187. Klinger, M.; Laske, C.; Graeve, M.; Thoma, M.; Traube, A. A Sensor for the In-Flight Detection of Single Fluorescent Microbodies in Nanoliter Droplets. *IEEE Sens. J.* **2020**, *20*, 5809–5817. [CrossRef]

188. Chen, X.; O'Mahony, A.P.; Barber, T. The characterization of particle number and distribution inside in-flight 3D printed droplets using a high speed droplet imaging system. *J. Appl. Phys.* **2021**, *130*, 044701. [CrossRef]
189. Chen, X.; O'Mahony, A.P.; Barber, T. The assessment of average cell number inside in-flight 3D printed droplets in microvalvebased bioprinting. *J. Appl. Phys.* **2022**, *131*, 224701. [CrossRef]
190. Engel, M.; Belfiore, L.; Aghaei, B.; Sutija, M. Enabling high throughput drug discovery in 3D cell cultures through a novel bioprinting workflow. *SLAS Technol.* **2022**, *27*, 32–38. [CrossRef]
191. Mallinson, S.; Barber, T.; Yeoh, G.; McBain, G. Simulation of droplet impact and spreading using a simple dynamic contact angle model. *Simulation* **2018**, *10*, 13.
192. Kang, S.H.; Kim, S.; Sohn, D.K.; Ko, H.S. Analysis of drop-ondemand piezo inkjet performance. *Phys. Fluids* **2020**, *32*, 022007. [CrossRef]
193. Xu, C.; Zhang, M.; Huang, Y.; Ogale, A.; Fu, J.; Markwald, R.R. Study of droplet formation process during drop-on-demand inkjetting of living cell-laden bioink. *Langmuir* **2014**, *30*, 9130–9138. [CrossRef] [PubMed]
194. Ng, W.L.; Yeong, W.Y.; Naing, M.W. Polyvinylpyrrolidone-based bio-ink improves cell viability and homogeneity during drop-ondemand printing. *Materials* **2017**, *10*, 190. [CrossRef] [PubMed]
195. Torrente-Rodríguez, R.M.; Tu, J.; Yang, Y.; Min, J.; Wang, M.; Song, Y.; Yu, Y.; Xu, C.; Ye, C.; IsHak, W.W.; et al. Investigation of cortisol dynamics in human sweat using a graphene-based wireless mhealth system. *Matter* **2020**, *2*, 921–937. [CrossRef]
196. Cen, C.; Wu, H.; Lee, C.-F.; Fan, L.; Liu, F. Experimental investigation on the sputtering and micro-explosion of emulsion fuel droplets during impact on a heated surface. *Int. J. Heat Mass Transf.* **2019**, *132*, 130–137. [CrossRef]
197. Mahmodi, H.; Piloni, A.; Utama, R.H.; Kabakova, I. Mechanical mapping of bioprinted hydrogel models by brillouin microscopy. *Bioprinting* **2021**, *23*, 00151. [CrossRef]
198. Wang, Q.; Lin, X.; Lin, Y.; Ma, J.; Xiao, J.; Wu, Y.; Wang, J. Effects of surface roughness on splashing characteristics of large droplets with digital inline holographic imaging. *Cold Reg. Sci. Technol.* **2021**, *191*, 103373. [CrossRef]
199. Quetzeri-Santiago, M.A.; Castrejón-Pita, A.A.; Castrejón-Pita, J.R. The effect of surface roughness on the contact line and splashing dynamics of impacting droplets. *Sci. Rep.* **2019**, *9*, 15030. [CrossRef]
200. Murphy, S.V.; Atala, A. 3D bioprinting of tissues and organs. *Nat. Biotechnol.* **2014**, *32*, 773–785. [CrossRef]
201. Chen, N.; Chen, H.; Amirfazli, A. Drop impact onto a thin film: Miscibility effect. *Phys. Fluids* **2017**, *29*, 092106. [CrossRef]
202. Yokoi, K. Numerical studies of droplet splashing on a dry surface: Triggering a splash with the dynamic contact angle. *Soft Matter* **2011**, *7*, 5120. [CrossRef]
203. Mundo, C.; Sommerfeld, M.; Tropea, C. Droplet-wall collisions: Experimental studies of the deformation and breakup process. *Int. J. Multiph. Flow* **1995**, *21*, 151–173. [CrossRef]
204. Gudapati, H.; Dey, M.; Ozbolat, I. A comprehensive review on droplet-based bioprinting: Past, present and future. *Biomaterials* **2016**, *102*, 20–42. [CrossRef] [PubMed]
205. Saygili, E.; Dogan-Gurbuz, A.A.; Yesil-Celiktas, O.; Draz, M.S. 3D bioprinting: A powerful tool to leverage tissue engineering and microbial systems. *Bioprinting* **2020**, *18*, 00071. [CrossRef]
206. Machekposhti, S.A.; Movahed, S.; Narayan, R.J. Physicochemical parameters that underlie inkjet printing for medical applications. *Biophys. Rev.* **2020**, *1*, 011301. [CrossRef]
207. Li, X.; Liu, B.; Pei, B.; Chen, J.; Zhou, D.; Peng, J.; Zhang, X.; Jia, W.; Xu, T. Inkjet bioprinting of biomaterials. *Chem. Rev.* **2020**, *120*, 10793–10833. [CrossRef]
208. Bejoy, A.M.; Makkithaya, K.N.; Hunakunti, B.B.; Hegde, A.; Krishnamurthy, K.; Sarkar, A.; Lobo, C.F.; Keshav, D.V.S.; Dharshini, G.; Mascarenhas, S.; et al. An insight on advances and applications of 3d bioprinting: A review. *Bioprinting* **2021**, *24*, 00176. [CrossRef]
209. Ouyang, L.; Yao, R.; Zhao, Y.; Sun, W. Effect of bioink properties on printability and cell viability for 3D bioplotting of embryonic stem cells. *Biofabrication* **2016**, *8*, 035020. [CrossRef]
210. Ng, W.L.; Lee, J.M.; Yeong, W.Y.; Win Naing, M. Microvalvebased bioprinting-process, bio-inks and applications. *Biomater. Sci.* **2017**, *5*, 632–647. [CrossRef]
211. Xu, H.; Casillas, J.; Xu, C. Effects of printing conditions on cell distribution within microspheres during inkjet-based bioprinting. *AIP Adv.* **2019**, *9*, 095055. [CrossRef]
212. Derakhshanfar, S.; Mbeleck, R.; Xu, K.; Zhang, X.; Zhong, W.; Xing, M. 3D bioprinting for biomedical devices and tissue engineering: A review of recent trends and advances. *Bioact. Mater* **2018**, *3*, 144–156. [CrossRef]
213. Chameettachal, S.; Yeleswarapu, S.; Sasikumar, S.; Shukla, P.; Hibare, P.; Bera, A.K.; Bojedla, S.S.R.; Pati, F. 3D Bioprinting: Recent trends and challenges. *J. Indian Inst. Sci.* **2019**, *99*, 375–403. [CrossRef]
214. Mobaraki, M.; Ghaffari, M.; Yazdanpanah, A.; Luo, Y.; Mills, D.K. Bioinks and bioprinting: A focused review. *Bioprinting* **2020**, *18*, e00080. [CrossRef]
215. Tan, Y.-C.; Cristini, V.; Lee, A.P. Monodispersed microfluidic droplet generation by shear focusing microfluidic device. *Sens. Actuators B Chem.* **2006**, *114*, 350–356. [CrossRef]
216. Motornov, M.; Minko, S.; Eichhorn, K.-J.; Nitschke, M.; Simon, F.; Stamm, M. Reversible tuning of wetting behaviour of polymer surface with responsive polymer brushes. *Langmuir* **2003**, *19*, 8077–8085. [CrossRef]
217. Galliker, P.; Schneider, J.; Eghlidi, H.; Kress, S.; Sandoghdar, V.; Poulikakos, D. Direct printing of nanostructures by electrostatic autofocussing of ink nanodroplets. *Nat. Commun.* **2012**, *3*, 890. [CrossRef]

218. Castrejon-Pita, J.R.; Baxter, W.R.S.; Morgan, J.; Temple, S.; Martin, G.D.; Hutchings, I.M. Future, opportunities and challenges of inkjet technologies. *At. Sprays* **2013**, *23*, 541–565. [CrossRef]
219. Bormashenko, E. *Wetting of Real Surfaces*; De Gruyter: Berlin, Germany, 2013.
220. Neumann, A.W.; Good, R.J. Thermodynamics of contact angles. I. Heterogeneous solid surfaces. *J. Colloid Interface Sci.* **1972**, *38*, 341–358. [CrossRef]
221. Marmur, A. Soft contact: Measurement and interpretation of contact angles. *Soft Matter* **2006**, *2*, 12–17. [CrossRef]
222. Calvert, P. Inkjet Printing for Materials and Devices. *Chem. Mater.* **2001**, *13*, 3299–3305. [CrossRef]
223. Gili, E.; Caironi, M.; Sirringhaus, H. Picoliter printing. In *Handbook of Nanofabrication*; Wiederrecht, G., Ed.; Elsevier: Amsterdam, The Netherlands, 2009; pp. 183–196.
224. Park, E.S. *Application of Inkjet-Printing Technology to Micro-Electro-Mechanical Systems*; University of California: Berkeley, CA, USA, 2014.
225. Modak, C.D.; Kumar, A.; Tripathy, A.; Sen, P. Drop impact printing. *Nat. Commun.* **2020**, *11*, 4327. [CrossRef]
226. Starly, B.; Shirwaiker, R. 3D bioprinting techniques. In *3D Bioprinting Nanotechnology in Tissue Engineering Regenerative Medicine*; Zhang, L.G., Fisher, J.P., Leong, K.W., Eds.; Elsevier: Amsterdam, The Netherlands, 2015; pp. 57–77.
227. Mandrycky, C.; Wang, Z.; Kim, K.; Kim, D.H. 3D bioprinting for engineering complex tissues. *Biotechnol. Adv.* **2016**, *34*, 422. [CrossRef] [PubMed]
228. Dasgupta, Q.; Black, L.D. A fresh slate for 3D bioprinting. *Science* **2019**, *365*, 446. [CrossRef] [PubMed]
229. Qu, J.; Dou, C.; Xu, B.; Li, J.; Rao, Z.; Tsin, A. Printing quality improvement for laser-induced forward transfer bioprinting: Numerical modeling and experimental validation. *Phys. Fluids* **2021**, *33*, 071906. [CrossRef]
230. Shin, P.; Sung, J.; Lee, M.H. Control of droplet formation for low viscosity fluid by double waveforms applied to a piezoelectric inkjet nozzle. *Microelectron. Reliab.* **2011**, *51*, 797–804. [CrossRef]
231. Lorenceau, É.; Quéré, D. Drops impacting a sieve. *J. Colloid Interface Sci.* **2003**, *263*, 244–249. [CrossRef]
232. Guo, Y.; Patanwala, H.S.; Bognet, B.; Ma, A.W.K. Inkjet and inkjet-based 3D printing: Connecting fluid properties and printing performance. *Rapid Prototyp. J.* **2017**, *23*, 562–576. [CrossRef]
233. Gao, M.; Li, L.; Song, Y. Inkjet printing wearable electronic devices. *J. Mater. Chem. C* **2017**, *5*, 2971–2993. [CrossRef]
234. Stadnytskyi, V.; Bax, C.E.; Bax, A.; Anfinrud, P. The airborne lifetime of small speech droplets and their potential importance in SARS-CoV-2 transmission. *Proc. Natl. Acad. Sci. USA* **2020**, *117*, 11875–11877. [CrossRef]
235. Jayaweera, M.; Perera, H.; Gunawardana, B.; Manatunge, J. Transmission of COVID-19 virus by droplets and aerosols: A critical review on the unresolved dichotomy. *Environ. Res.* **2020**, *188*, 109819. [CrossRef]
236. Melayil, K.R.; Mitra, S.K. Wetting, adhesion, and droplet impact on face masks. *Langmuir* **2021**, *37*, 2810–2815. [CrossRef]
237. World Health Organization. *Advice on the Use of Masks in the Context of COVID-19*; World Health Organization: Geneva, Switzerland, 2020.
238. Katre, P.; Banerjee, S.; Balusamy, S.; Sahu, K.C. Fluid dynamics of respiratory droplets in the context of COVID-19: Airborne and surfaceborne transmissions. *Phys. Fluids* **2021**, *33*, 081302. [CrossRef] [PubMed]
239. Hetherington, R.; Hasan, A.B.M.T.; Khan, A.; Roy, D.; Salehin, M.; Wadud, Z. Exposure risk analysis of COVID-19 for a ride-sharing motorbike taxi. *Phys. Fluids* **2021**, *33*, 113319. [CrossRef] [PubMed]
240. Bhardwaj, R.; Agrawal, A. Likelihood of survival of coronavirus in a respiratory droplet deposited on a solid surface. *Phys. Fluids* **2020**, *32*, 061704. [CrossRef] [PubMed]
241. Kumar, B.; Chatterjee, S.; Agrawal, A.; Bhardwaj, R. Evaluating a transparent coating on a face shield for repelling airborne respiratory droplets. *Phys. Fluids* **2021**, *33*, 111705. [CrossRef] [PubMed]
242. Shafaghi, A.H.; Talabazar, F.R.; Kosar, A.; Ghorbani, M. On the effect of the respiratory droplet generation condition on COVID-19 transmission. *Fluids* **2020**, *5*, 113. [CrossRef]
243. Mittal, R.; Ni, R.; Seo, J.-H. The flow physics of COVID-19. *J. Fluid Mech.* **2020**, *894*, F2. [CrossRef]
244. Poon, W.C.K.; Brown, A.T.; Direito, S.O.L.; Hodgson, D.J.M.; Nagard, L.L.; Lips, A.; MacPhee, C.E.; Marenduzzo, D.; Royer, J.R.; Silva, A.F.; et al. Soft matter science and the COVID-19 pandemic. *Soft Matter* **2020**, *16*, 8310–8324. [CrossRef]
245. Liao, M.; Liu, H.; Wang, X.; Hu, X.; Huang, Y.; Liu, X.; Brenan, K.; Mecha, J.; Nirmalan, M.; Lu, J.R. A technical review of face mask wearing in preventing respiratory COVID-19 transmission. *Curr. Opin. Colloid Interface Sci.* **2021**, *52*, 101417. [CrossRef]
246. Meier, W.; Greune, G.; Meyboom, A.; Hofmann, K.P. Surface tension and viscosity of surfactant from the resonance of an oscillating drop. *Eur. Biophys. J.* **2000**, *29*, 113–124. [CrossRef]
247. Wijshoff, H. The dynamics of the piezo inkjet printhead operation. *Phys. Rep.* **2010**, *491*, 77–177. [CrossRef]
248. Bostwick, J.B.; Steen, P.H. Dynamics of sessile drops. Part 1. Inviscid theory. *J. Fluid Mech.* **2014**, *760*, 5–38. [CrossRef]
249. Mohammad Karim, A. Parametric Study of Liquid Contact Line Dynamics: Adhesion vs. Hydrodynamics. Ph.D. Thesis, UCLA, Los Angeles, CA, USA, 2015.
250. Mohammad Karim, A.; Fujii, K.; Kavehpour, H.P. Contact line dynamics of gravity driven spreading of liquids. *Fluid Dyn. Res.* **2021**, *53*, 035503. [CrossRef]
251. Mohammad Karim, A.; Suszynski, W.J.; Pujari, S. Liquid Film Stability and Contact Line Dynamics of Emulsion Liquid Films in Curtain Coating Process. *J. Coat. Technol. Res.* **2021**, *18*, 1531–1541. [CrossRef]
252. Abe, Y.; Zhang, B.; Gordillo, L.; Mohammad Karim, A.; Francis, L.F.; Cheng, X. Dynamic self-assembly of charged colloidal strings and walls in simple fluid flows. *Soft Matter* **2017**, *13*, 1681–1692. [CrossRef] [PubMed]

253. Almohammadi, H.; Amirfazli, A. Droplet impact: Viscosity and wettability effects on splashing. *J. Colloid Interf. Sci.* **2019**, *553*, 22–30. [CrossRef] [PubMed]
254. Kavehpour, H.P.; Mohammad Karim, A.; Davis, S.H. Inconsistencies in the experimental study of spontaneous spreading vs. forced spreading. In *Proceedings of the Droplets 2015*; University of Twente: Enschede, The Netherlands, 2015.
255. Ebert, J.; Özkol, E.; Zeichner, A.; Uibel, K.B.; Weiss, Ö.; Koops, U.; Telle, R.; Fischer, H. Direct inkjet printing of dental prostheses made of zirconia. *J. Dent. Res.* **2009**, *88*, 673–676. [CrossRef] [PubMed]
256. Jonczyk, R.; Kurth, T.; Lavrentieva, A.; Walter, J.-G.; Scheper, T.; Stahl, F. Living cell microarrays: An overview of concepts. *Microarrays* **2016**, *5*, 11. [CrossRef]
257. Liu, Y.; Derby, B. Experimental study of the parameters for stable drop-on-demand inkjet performance. *Phys. Fluids* **2019**, *31*, 032004. [CrossRef]
258. Derby, B. Inkjet printing of functional and structural materials: Fluid property requirements, feature stability, and resolution. *Annu. Rev. Mater. Res.* **2010**, *40*, 395–414. [CrossRef]
259. Gong, Y.; Bi, Z.; Bian, X.; Ge, A.; He, J.; Li, W.; Shao, H.; Chen, G.; Zhang, X. Study on linear bio-structure print process based on alginate bio-ink in 3D bio-fabrication. *Bio-Des. Manuf.* **2020**, *3*, 109–121. [CrossRef]
260. Libanori, A.; Chen, G.; Zhao, X.; Zhou, Y.; Chen, J. Smart textiles for personalized healthcare. *Nat. Electron.* **2022**, *5*, 142–156. [CrossRef]
261. Gao, W.; Emaminejad, S.; Nyein, H.Y.Y.; Challa, S.; Chen, K.; Peck, A.; Fahad, H.M.; Ota, H.; Shiraki, H.; Kiriya, D.; et al. Fully integrated wearable sensor arrays for multiplexed in situ perspiration analysis. *Nature* **2016**, *529*, 509–514. [CrossRef] [PubMed]
262. Kim, J.; Campbell, A.; de Ávila, B.; Wang, J. Wearable biosensors for healthcare monitoring. *Nat. Biotechnol.* **2019**, *37*, 389–406. [CrossRef] [PubMed]
263. Ates, H.; Nguyen, P.; Gonzalez-Macia, L.; Morales-Narvez, E.; Güder, F.; Collins, J.; Dincer, C. End-to-end design of wearable sensors. *Nat. Rev. Mater.* **2022**, *7*, 887–907. [CrossRef]
264. Xu, C.; Yang, Y.; Gao, W. Skin-interfaced sensors in digital medicine: From materials to applications. *Matter* **2020**, *2*, 1414–1445. [CrossRef]
265. Heikenfeld, J.; Jajack, A.; Feldman, B.; Granger, S.; Gaitonde, S.; Begtrup, G.; Katchman, B. Accessing analytes in biofluids for peripheral biochemical monitoring. *Nat. Biotechnol.* **2019**, *37*, 407–419. [CrossRef]
266. Someya, T.; Bao, Z.; Malliaras, G.G. The rise of plastic bioelectronics. *Nature* **2016**, *540*, 379–385. [CrossRef]
267. Bandodkar, A.J.; Jeang, W.J.; Ghaffari, R.; Rogers, J.A. Wearable sensors for biochemical sweat analysis. *Annu. Rev. Anal. Chem.* **2019**, *12*, 1–22. [CrossRef]
268. Wang, M.; Yang, Y.; Min, J.; Song, Y.; Tu, J.; Mukasa, D.; Ye, C.; Xu, C.; Heflin, N.; McCune, J.; et al. Awearable electrochemical biosensor for the monitoring of metabolites and nutrients. *Nat. Biomed. Eng.* **2022**, *6*, 1225–1235. [CrossRef]
269. Shikhmurzaev, Y. The Moving Contact Line on a Smooth Solid Surface. *Int. J. Multiph. Flow* **1993**, *19*, 589–610. [CrossRef]
270. Shikhmurzaev, Y.D. Mathematical Modeling of Wetting Hydrodynamics. *Fluid Dyn. Res.* **1994**, *13*, 45–64. [CrossRef]
271. Shikhmurzaev, Y.D. Moving Contact Lines in Liquid/Liquid/Solid Systems. *J. Fluid Mech.* **1997**, *334*, 211–249. [CrossRef]
272. Moghtadernejad, S.; Lee, C.; Jadidi, M. An introduction of droplet impact dynamics to engineering students. *Fluids* **2020**, *5*, 107. [CrossRef]
273. Thoroddsen, S.T.; Etoh, T.G.; Takehara, K. High-speed imaging of drops and bubbles. *Annu. Rev. Fluid Mech.* **2008**, *40*, 257–285. [CrossRef]
274. Worthington, A.M. On the forms assumed by drops of liquids falling vertically on a horizontal plate. *Proc. R. Soc.* **1876**, *25*, 261–272.
275. Cheng, X.; Sun, T.-P.; Gordillo, L. Drop impact dynamics: Impact force and stress distributions. *Annu. Rev. Fluid Mech.* **2022**, *54*, 57–81. [CrossRef]
276. Chen, L.; Bonaccurso, E.; Deng, P.; Zhang, H. Droplet impact on soft viscoelastic surfaces. *Phys. Rev. E* **2016**, *94*, 063117. [CrossRef]
277. Saiki, Y.; Prestidge, C.A.; Horn, R.G. Effects of droplet deformability on emulsion rheology. *Colloids Surf. A* **2006**, *299*, 65. [CrossRef]
278. Lester, G.R. Contact angles of liquids at deformable solid surfaces. *J. Colloid Sci.* **1961**, *16*, 315. [CrossRef]
279. Blanken, N.; Saleem, M.S.; Thoraval, M.-J.; Antonini, C. Impact of compound drops: A perspective. *Curr. Opin. Colloid Interface Sci.* **2021**, *51*, 101389. [CrossRef]
280. Lee, J.B.; dos Santos, S.; Antonini, C. Water touch-and-bounce from a soft viscoelastic substrate: Wetting, dewetting, and rebound on bitumen. *Langmuir* **2016**, *32*, 8245–8254. [CrossRef] [PubMed]
281. Langley, K.R.; Castrejón-Pita, A.A.; Thoroddsen, S.T. Droplet impacts onto soft solids entrap more air. *Soft Matter* **2020**, *16*, 5702–5710. [CrossRef]
282. Chen, S.; Bertola, V. Drop impact on spherical soft surfaces. *Phys. Fluids* **2017**, *29*, 082106. [CrossRef]
283. Poulain, S.; Carlson, A. Droplet settling on solids coated with a soft layer. *J. Fluid Mech.* **2022**, *934*, A25. [CrossRef]
284. Skotheim, J.M.; Mahadevan, L. Soft lubrication: The elastohydrodynamics of nonconforming and conforming contacts. *Phys. Fluids* **2005**, *17*, 092101. [CrossRef]
285. Essink, M.H.; Pandey, A.; Karpitschka, S.; Venner, C.H.; Snoeijer, J.H. Regimes of soft lubrication. *J. Fluid Mech.* **2021**, *915*, A49. [CrossRef]

286. Wang, Y.; Pilkington, G.A.; Dhong, C.; Frechette, J. Elastic deformation during dynamic force measurements in viscous fluids. *Curr. Opin. Colloid Interface Sci.* **2017**, *27*, 43–49. [CrossRef]
287. Chan, T.S.; Carlson, A. Physics of adhesive organs in animals. *Eur. Phys. J. Spec. Top.* **2019**, *227*, 2501–2512. [CrossRef]
288. Pepper, R.E.; Courbin, L.; Stone, H.A. Splashing on elastic membranes: The importance of early-time dynamics. *Phys. Fluids* **2008**, *20*, 082103. [CrossRef]
289. Arai, K.; Iwanaga, S.; Toda, H.; Genci, C.; Nishiyama, Y.; Nakamura, M. Three-dimensional inkjet biofabrication based on designed images. *Biofabrication* **2011**, *3*, 34113. [CrossRef]
290. Andreotti, B.; Snoeijer, J.H. Statics and dynamics of soft wetting. *Annu. Rev. Fluid Mech.* **2020**, *52*, 285–308. [CrossRef]
291. Dervaux, J.; Roché, M.; Limat, L. Nonlinear theory of wetting on deformable substrates. *Soft Matter* **2020**, *16*, 5157–5176. [CrossRef] [PubMed]
292. Rioboo, R.; Voue, M.; Adao, H.; Conti, J.; Vaillant, A.; Seveno, D.; De Coninck, J. Drop impact on soft surfaces: Beyond the static contact angles. *Langmuir* **2010**, *26*, 4873–4879. [CrossRef] [PubMed]
293. Brochard-Wyart, F.; de Gennes, P. Dynamics of Partial Wetting. *Adv. Colloid Interface Sci.* **1992**, *39*, 1–11. [CrossRef]
294. Alizadeh, A.; Bahadur, V.; Shang, W.; Zhu, Y.; Buckley, D.; Dhinojwala, A.; Sohal, M. Influence of substrate elasticity on droplet impact dynamics. *Langmuir* **2013**, *29*, 4520–4524. [CrossRef]
295. Mangili, S.; Antonini, C.; Marengo, M.; Amirfazli, A. Understanding the drop impact phenomenon on soft PDMS substrates. *Soft Matter* **2012**, *8*, 10045. [CrossRef]
296. Pericet-Camara, R.; Auernhammer, G.K.; Koynov, K.; Lorenzoni, S.; Raiteri, R.; Bonnacurso, E. Solid-supported thin elastomer films deformed by microdrops. *Soft Matter* **2009**, *5*, 3611–3617. [CrossRef]
297. Kern, R.; Müller, P. Deformation of an elastic thin solid induced by a liquid droplet. *Surf. Sci.* **1992**, *264*, 467–494. [CrossRef]
298. Yu, Y.; Zhao, Y. Elastic deformation of soft membrane with finite thickness induced by a sessile liquid droplet. *J. Colloid Interface Sci.* **2009**, *339*, 489–494. [CrossRef]
299. Gerber, J.; Schutzius, T.M.; Poulikakos, D. Patterning of colloidal droplet deposits on soft materials. *J. Fluid Mech.* **2021**, *907*, A39. [CrossRef]
300. Liu, Y.; Ma, L.; Wang, W.; Kota, A.K.; Hu, H. An experimental study on soft PDMS materials for aircraft icing mitigation. *Appl. Surf. Sci.* **2018**, *447*, 599–609. [CrossRef]
301. Dressaire, E.; Sauret, A.; Boulogne, F.; Stone, H.A. Drop impact on a flexible fiber. *Soft Matter* **2016**, *12*, 200–208. [CrossRef] [PubMed]
302. Li, N.; Zhou, Q.; Chen, X.; Xu, T.; Hui, S.; Zhang, D. Liquid drop impact on solid surface with application to water drop erosion on turbine blades, Part I: Nonlinear wave model and solution of one-dimensional impact. *Int. J. Mech. Sci.* **2008**, *50*, 1526–1542. [CrossRef]
303. Adler, W.F. Waterdrop impact modeling. *Wear* **1995**, *186–187*, 341–351. [CrossRef]
304. Bico, J.; Reyssat, É.; Roman, B. Elastocapillarity: When surface tension deforms elastic solids. *Annu. Rev. Fluid Mech.* **2018**, *50*, 629–659. [CrossRef]
305. de Goede, T.C.; Moqaddam, A.M.; Limpens, K.C.M.; Kooij, S.A.; Derome, D.; Carmeliet, J.; Shahidzadeh, N.; Bonn, D. Droplet impact of Newtonian fluids and blood on simple fabrics: Effect of fabric pore size and underlying substrate. *Phys. Fluids* **2021**, *33*, 033308. [CrossRef]
306. Banitabaei, S.A.; Amirfazli, A. Droplet impact onto a solid sphere: Effect of wettability and impact velocity. *Phys. Fluids* **2017**, *29*, 062111. [CrossRef]
307. Faulkner-Jones, A.; Greenhough, S.; A King, J.; Gardner, J.; Courtney, A.; Shu, W. Development of a valve-based cell printer for the formation of human embryonic stem cell spheroid aggregates. *Biofabrication* **2013**, *5*, 15013. [CrossRef]
308. Soto, D.; De Larivière, A.B.; Boutillon, X.; Clanet, C.; Quéré, D. The force of impacting rain. *Soft Matter* **2014**, *10*, 4929. [CrossRef]
309. Gart, S.; Mates, J.E.; Megaridis, C.M.; Jung, S. Droplet impacting a cantilever: A leaf–raindrop system. *Phys. Rev. Appl.* **2015**, *3*, 044019. [CrossRef]
310. Dong, X.; Huang, X.; Liu, J. Modeling and simulation of droplet impact on elastic beams based on SPH. *Eur. J. Mech. A Solids* **2019**, *75*, 237–257. [CrossRef]
311. Huang, X.; Dong, X.; Li, J.; Liu, J. Droplet impact induced large deflection of a cantilever. *Phys. Fluids* **2019**, *31*, 062106. [CrossRef]
312. Ray, T.; Choi, J.; Bandodkar, A.; Krishnan, S.; Gutruf, P.; Tian, L.; Ghaffari, R.; Rogers, J. Bio-integrated wearable systems: A comprehensive review. *Chem. Rev.* **2019**, *119*, 5461–5533. [CrossRef] [PubMed]
313. Chen, F.; Song, J.; Lu, Y.; Huang, S.; Liu, X.; Sun, J.; Carmalt, C.J.; Parkin, I.P.; Xu, W. Creating robust superamphiphobic coatings for both hard and soft materials. *J. Mater. Chem. A.* **2015**, *3*, 20999–21008. [CrossRef]
314. Yang, Y.; Gao, W. Wearable and flexible electronics for continuous molecular monitoring. *Chem. Soc. Rev.* **2019**, *48*, 1465–1491. [CrossRef] [PubMed]
315. Jia, W.; Bandodkar, A.J.; Vald´ es-Ramírez, G.; Windmiller, J.R.; Yang, Z.; Ramírez, J.; Chan, G.; Wang, J. Electrochemical tattoo biosensors for real-time noninvasive lactate monitoring in human perspiration. *Anal. Chem.* **2013**, *85*, 6553–6560. [CrossRef]
316. Jia, W.; Vald´ es-Ramírez, G.; Bandodkar, A.J.; Windmiller, J.R.; Wang, J. Epidermal Biofuel Cells: Energy Harvesting from Human Perspiration. *Angew. Chem. Int. Ed.* **2013**, *52*, 7233–7236. [CrossRef]
317. Lv, J.; Jeerapan, I.; Tehrani, F.; Yin, L.; Silva-Lopez, C.A.; Jang, J.H.; Joshuia, D.; Shah, R.; Liang, Y.; Xie, L.; et al. Sweat-based wearable energy harvesting-storage hybrid textile devices. *Energy Environ. Sci.* **2018**, *11*, 3431–3442. [CrossRef]

318. Yang, Y.; Song, Y.; Bo, X.; Min, J.; Pak, O.S.; Zhu, L.; Wang, M.; Tu, J.; Kogan, A.; Zhang, H.; et al. A laser-engraved wearable sensor for sensitive detection of uric acid and tyrosine in sweat. *Nat. Biotechnol.* **2020**, *38*, 217–224. [CrossRef]
319. Pal, A.; Goswami, D.; Cuellar, H.E.; Castro, B.; Kuang, S.; Martinez, R.V. Early detection and monitoring of chronic wounds using low-cost, omniphobic paper-based smart bandages. *Biosens. Bioelectron.* **2018**, *117*, 696–705. [CrossRef]
320. Gao, W.; Nyein, H.Y.Y.; Shahpar, Z.; Fahad, H.M.; Chen, K.; Emaminejad, S.; Gao, Y.; Tai, L.C.; Ota, H.; Wu, E.; et al. Wearable microsensor array for multiplexed heavy metal monitoring of body fluids. *ACS Sens.* **2016**, *1*, 866–874. [CrossRef]
321. Yu, Y.; Nyein, H.Y.Y.; Gao, W.; Javey, A. Flexible electrochemical bioelectronics: The rise of in situ bioanalysis. *Adv. Mater.* **2020**, *32*, 1902083. [CrossRef] [PubMed]
322. Yu, Y.; Nassar, J.; Xu, C.; Min, J.; Yang, Y.; Dai, A.; Doshi, R.; Huang, A.; Song, Y.; Gehlhar, R.; et al. Biofuel-powered soft electronic skin with multiplexed and wireless sensing for human-machine interfaces. *Sci. Robot.* **2020**, *5*, eaaz7946. [CrossRef] [PubMed]
323. Rose, D.P.; Ratterman, M.; Griffin, D.K.; Hou, L.; Kelley-Loughnane, N.; Naik, R.K.; Hagen, J.A.; Papautsky, I.; Heikenfeld, J. System-level design of an RFID sweat electrolyte sensor patch. In Proceedings of the 2014 36th Annual International Conference of the IEEE Engineering in Medicine and Biology Society, EMBC 2014, Chicago, IL, USA, 26–30 August 2014; IEEE: Piscataway, NJ, USA, 2014; pp. 4038–4041.
324. Rose, D.P.; Ratterman, M.E.; Griffin, D.K.; Hou, L.; Kelley-Loughnane, N.; Naik, R.R.; Hagen, J.A.; Papautsky, I.; Heikenfeld, J.C. Adhesive RFID sensor patch for monitoring of sweat electrolytes. *IEEE Trans. Biomed. Eng.* **2015**, *62*, 1457–1465. [CrossRef] [PubMed]
325. Bandodkar, A.J.; Gutruf, P.; Choi, J.; Lee, K.H.; Sekine, Y.; Reeder, J.T.; Jeang, W.J.; Aranyosi, A.J.; Lee, S.P.; Model, J.B.; et al. Battery-free, skin-interfaced microfluidic/electronic systems for simultaneous electrochemical, colorimetric, and volumetric analysis of sweat. *Sci. Adv.* **2019**, *5*, eaav3294. [CrossRef]
326. Bandodkar, A.J.; Hung, V.W.S.; Jia, W.; Vald´ es-Ramírez, G.; Windmiller, J.R.; Martinez, A.G.; Ramírez, J.; Chan, G.; Kerman, K.; Wang, J. Tattoo-based potentiometric ion-selective sensors for epidermal pH monitoring. *Analyst* **2013**, *138*, 123–128. [CrossRef]
327. Bandodkar, A.J.; Jia, W.; Yardimci, C.; Wang, X.; Ramirez, J.; Wang, J. Tattoo-based noninvasive glucose monitoring: A proof-of-concept study. *Anal. Chem.* **2015**, *87*, 394–398. [CrossRef]
328. Bandodkar, A.J.; O'Mahony, A.M.; Ramírez, J.; Samek, I.A.; Anderson, S.M.; Windmiller, J.R.; Wang, J. Solid-state forensic finger sensor for integrated sampling and detection of gunshot residue and explosives: Towards Lab-on-a-finger. *Analyst* **2013**, *138*, 5288–5295. [CrossRef]
329. Kagie, A.; Bishop, D.K.; Burdick, J.; La Belle, J.T.; Dymond, R.; Felder, R.; Wanga, J. Flexible rolled thick-film miniaturized flow-cell for minimally invasive amperometric sensing. *Electroanalysis* **2008**, *20*, 1610–1614. [CrossRef]
330. Sempionatto, J.R.; Brazaca, L.C.; García-Carmona, L.; Bolat, G.; Campbell, A.S.; Martin, A.; Tang, G.; Shah, R.; Mishra, R.K.; Kim, J.; et al. Eyeglasses-based tear biosensing system: Non-invasive detection of alcohol, vitamins and glucose. *Biosens. Bioelectron.* **2019**, *137*, 161–170. [CrossRef]
331. Sempionatto, J.R.; Itthipon, I.; Krishnan, S.; Wang, J. Wearable chemical sensors: Emerging systems for on-body analytical chemistry. *Anal. Chem.* **2019**, *92*, 378–396. [CrossRef] [PubMed]
332. Sempionatto, J.R.; Khorshed, A.A.; Ahmed, A.; De Loyola E Silva, A.N.; Barfidokht, A.; Yin, L.; Goud, K.Y.; Mohamed, M.A.; Bailey, E.; May, J.; et al. Epidermal enzymatic biosensors for sweat vitamin C: Toward personalized nutrition. *ACS Sens.* **2020**, *5*, 1804–1813. [CrossRef] [PubMed]
333. Kim, J.; De Araujo, W.R.; Samek, I.A.; Bandodkar, A.J.; Jia, W.; Brunetti, B.; Paixão, T.R.L.C.; Wang, J. Wearable temporary tattoo sensor for real-time trace metal monitoring in human sweat. *Electrochem. Commun.* **2015**, *51*, 41–45. [CrossRef]
334. Kim, J.; Imani, S.; de Araujo, W.R.; Warchall, J.; Valdés-Ramírez, G.; Paixão, T.R.L.C.; Mercier, P.P.; Wang, J. Wearable salivary uric acid mouthguard biosensor with integrated wireless electronics. *Biosens. Bioelectron.* **2015**, *74*, 1061–1068. [CrossRef]
335. García-Carmona, L.; Martín, A.; Sempionatto, J.R.; Moreto, J.R.; González, M.C.; Wang, J.; Escarpa, A. Pacifier biosensor: Toward noninvasive saliva biomarker monitoring. *Anal. Chem.* **2019**, *91*, 13883–13891. [CrossRef]
336. Sempionatto, J.R.; Mishra, R.K.; Martín, A.; Tang, G.; Nakagawa, T.; Lu, X.; Campbell, A.S.; Lyu, K.M.; Wang, J. Wearable ring-based sensing platform for detecting chemical threats. *ACS Sens.* **2017**, *2*, 1531–1538. [CrossRef]
337. Sempionatto, J.R.; Nakagawa, T.; Pavinatto, A.; Mensah, S.T.; Imani, S.; Mercier, P.; Wang, J. Eyeglasses based wireless electrolyte and metabolite sensor platform. *Lab Chip* **2017**, *17*, 1834–1842. [CrossRef]
338. Ciui, B.; Martin, A.; Mishra, R.K.; Brunetti, B.; Nakagawa, T.; Dawkins, T.J.; Lyu, M.; Cristea, C.; Sandulescu, R.; Wang, J. Wearable wireless tyrosinase bandage and microneedle sensors: Toward melanoma screening. *Adv. Healthc. Mater.* **2018**, *7*, 1701264. [CrossRef]

Disclaimer/Publisher's Note: The statements, opinions and data contained in all publications are solely those of the individual author(s) and contributor(s) and not of MDPI and/or the editor(s). MDPI and/or the editor(s) disclaim responsibility for any injury to people or property resulting from any ideas, methods, instructions or products referred to in the content.